Circulation

ORIGINAL RESEARCH ARTICLE

Nuclear Receptor NR1D1 Regulates Abdominal Aortic Aneurysm Development by Targeting the Mitochondrial Tricarboxylic Acid Cycle Enzyme Aconitase-2

Ling-Yue Sun, MS*; Yu-Yan Lyu, MD, PhD*; Heng-Yuan Zhang, MS; Zhi Shen, BS; Guan-Qiao Lin, BS; Na Geng, BS; Yu-Li Wang, BS; Lin Huang, PhD; Ze-Hao Feng, MS; Xiao Guo, PhD; Nan Lin, MS; Song Ding, MD, PhD; An-Cai Yuan, MD, PhD; Lan Zhang, MD, PhD; Kun Qian, PhD; Jun Pu, MD, PhD

BACKGROUND: Metabolic disorder increases the risk of abdominal aortic aneurysm (AAA). NRs (nuclear receptors) have been increasingly recognized as important regulators of cell metabolism. However, the role of NRs in AAA development remains largely unknown.

METHODS: We analyzed the expression profile of the NR superfamily in AAA tissues and identified NR1D1 (NR subfamily 1 group D member 1) as the most highly upregulated NR in AAA tissues. To examine the role of NR1D1 in AAA formation, we used vascular smooth muscle cell (VSMC)–specific, endothelial cell–specific, and myeloid cell–specific conditional *Nr1d1* knockout mice in both AngII (angiotensin II)– and $CaPO_4$-induced AAA models.

RESULTS: *Nr1d1* gene expression exhibited the highest fold change among all 49 NRs in AAA tissues, and NR1D1 protein was upregulated in both human and murine VSMCs from AAA tissues. The knockout of *Nr1d1* in VSMCs but not endothelial cells and myeloid cells inhibited AAA formation in both AngII- and $CaPO_4$-induced AAA models. Mechanistic studies identified ACO2 (aconitase-2), a key enzyme of the mitochondrial tricarboxylic acid cycle, as a direct target trans-repressed by NR1D1 that mediated the regulatory effects of NR1D1 on mitochondrial metabolism. NR1D1 deficiency restored the ACO2 dysregulation and mitochondrial dysfunction at the early stage of AngII infusion before AAA formation. Supplementation with αKG (α-ketoglutarate, a downstream metabolite of ACO2) was beneficial in preventing and treating AAA in mice in a manner that required NR1D1 in VSMCs.

CONCLUSIONS: Our data define a previously unrecognized role of nuclear receptor NR1D1 in AAA pathogenesis and an undescribed NR1D1-ACO2 axis involved in regulating mitochondrial metabolism in VSMCs. It is important that our findings suggest αKG supplementation as an effective therapeutic approach for AAA treatment.

Key Words: alpha-Ketoglutarate ■ abdominal aortic aneurysm ■ mitochondria ■ nuclear receptor ■ vascular smooth muscle

Abdominal aortic aneurysm (AAA) is a life-threatening disease characterized by permanent regional dilation of the abdominal aorta, resulting in catastrophic events of rupture and sudden death.[1] The majority of patients with AAA are asymptomatic until lethal rupture, which impedes AAA diagnosis at an early stage.[1] At

Correspondence to: Jun Pu, MD, PhD, Department of Cardiology, Renji Hospital, School of Medicine, State Key Laboratory for Oncogenes and Related Genes, Shanghai Cancer Institute, Shanghai Jiao Tong University, 160 Pujian Road, Shanghai 200127, China. Email pujun310@hotmail.com

*L.-Y. Sun and Y.-Y. Lyu contributed equally.

Supplemental Material is available at https://www.ahajournals.org/doi/suppl/10.1161/CIRCULATIONAHA.121.057623.

For Sources of Funding and Disclosures, see page 1608.

ORIGINAL RESEARCH ARTICLE

Clinical Perspective

What Is New?

- NR1D1 (Nuclear receptor subfamily 1 group D member 1) ranks the highest in fold change among all 49 nuclear receptors in abdominal aortic aneurysm (AAA) tissues, and global or vascular smooth muscle cell–specific knockout of *Nr1d1* represses AAA formation.
- Mitochondrial tricarboxylic acid cycle enzyme ACO2 (aconitase-2) is identified as a direct target transrepressed by NR1D1 that mediates the regulatory effects of NR1D1 on mitochondrial metabolism.
- Our study unveils a previously undescribed NR1D1-ACO2-αKG (α-ketoglutarate) axis in regulating mitochondrial metabolism and AAA pathogenesis, and provides proof-of-concept evidence indicating the therapeutic value of αKG (a metabolite of the tricarboxylic acid cycle) in AAA prevention and treatment.

What Are the Clinical Implications?

- αKG is a biological compound found naturally in the human body and available in dietary supplement form, allowing for rapid clinical translation.
- On the basis of these findings, a prospective and randomized study (Alpha-Ketoglutarate in Abdominal Aortic Aneurysm, 4A Study; Registration: https://www.clinicaltrials.gov; Unique identifier: NCT04723888) to assess the efficacy and safety of αKG in patients with AAA has been initiated.

Nonstandard Abbreviations and Acronyms

AAA	abdominal aortic aneurysm
ACO2	aconitase-2
αKG	α-ketoglutarate
AngII	angiotensin II
DM-αKG	dimethyl α-ketoglutarate
ETC	electron transport chain
HDAC3	histone deacetylase 3
IL-6	interleukin-6
MASMC	mouse aortic smooth muscle cell
MCP-1	monocyte chemoattractant protein-1
MMP	matrix metallopeptidase
mtDNA	mitochondrial DNA
NCoR1	nuclear receptor corepressor 1
NR	nuclear receptor
NR1D1	nuclear receptor subfamily 1 group D member 1
RT-qPCR	real-time quantitative polymerase chain reaction
TCA	tricarboxylic acid
TNF-α	tumor necrosis factor-α
VSMC	vascular smooth muscle cell

present, open surgical repair and endovascular placement of a stent graft are the mainstays of treatment for AAA, and there are no US Food and Drug Administration–approved medical therapies to limit the progression or reduce the risk of rupture.[1] To identify novel therapeutic targets, a profound understanding of the underlying molecular mechanism regulating AAA formation and progression is essential.

Metabolic pathways, including glucose metabolism, lipid metabolism, and amino acid metabolism, have indispensable roles in normal and dysfunctional vasculature.[2] As the powerhouse of cells, mitochondria play a fundamental role in regulating these metabolic pathways through the tricarboxylic acid (TCA) cycle and oxidative phosphorylation, and tight control of mitochondrial functions is critical to maintaining metabolic homeostasis.[3] A recent single-cell RNA sequencing study demonstrated that extensive mitochondrial dysfunction occurs in different aortic cell types and is a feature of aortic aneurysms;[4] however, the regulatory mechanisms of mitochondrial metabolic pathways in aortic aneurysm development remain poorly understood.

Metabolic nuclear receptors (NRs) are a class of ligand-inducible transcription factors that regulate gene expression during various physiological/pathological processes, especially basal metabolic function and energy metabolism.[5,6] Several members of this superfamily have been demonstrated to be present in the vasculature, with important roles in vascular physiology/pathology. NR1D1 (NR subfamily 1 group D member 1), also known as Rev-erbα, belongs to the NR superfamily, which was first cloned in pituitary tissue and recognized as a vital regulator of circadian rhythms.[7–9] Recently, several new functions of NR1D1 beyond its roles in circadian rhythms were identified (ie, regulating cell metabolism and inflammatory responses) and implicated in the pathogenesis of several metabolic diseases[10,11] and cardiovascular diseases.[8,9,12,13] Although NR1D1 has recently been demonstrated to be expressed in vascular cells, the functional role of NR1D1 in the pathology of AAA has never been investigated.

In this study, we aimed to investigate whether NR1D1 is involved in the pathogenesis of AAA and explore the underlying mechanisms. We report our findings that vascular smooth muscle cell (VSMC)-derived NR1D1 contributes to AAA formation by targeting the mitochondrial TCA cycle enzyme ACO2 (aconitase-2). Moreover, αKG (α-ketoglutarate), a downstream metabolite of ACO2, rescued mitochondrial dysfunction and restricted AAA formation.

METHODS

The data that support the findings of this study are available from the corresponding author on reasonable request.

Human Studies

All human samples used in this study were processed under protocols approved by the institutional review board at Shanghai Jiao Tong University. All study participants were recruited after providing informed consent with approval by the Ethics Committee of Renji Hospital, School of Medicine, Shanghai Jiao Tong University; and the study was conducted according to the criteria set by the Declaration of Helsinki (2013).

Human AAA tissue samples were obtained from 6 patients undergoing surgical repair for AAA from December 1, 2018, to March 1, 2019 (Table S1). Tissues were sampled in the morning (8 AM to 10 AM). All patients were recruited from patients with abdominal aortic diameters ≥55 mm measured by computed tomographic angiography. The 2018 Society of Vascular Surgery Practice Guidelines on the care of patients with AAA recommend elective repair for patients at low or acceptable surgical risk with a fusiform AAA ≥55 mm.[1] Adjacent nonaneurysmal aortic segments (non-AAA) were obtained from the same patient and used as controls.

In another series of studies, plasma samples were collected from 40 study participants (20 patients with AAA and 20 matched controls) from May 4, 2020, to October 15, 2020. Patients with AAA were recruited from a pool of patients undergoing computed tomographic angiography to assess AAA morphometry in accordance with the Society for Vascular Surgery Practice Guidelines.[1] AAA is defined as an enlargement of the abdominal aorta to ≥30 mm in diameter.[1] To avoid possible interference by other confounding factors on the metabolomic profiling, we included patients with AAA only in the age range of 50 to 75 years and excluded patients from the study if they had (1) genetic aortic disease, autoimmune or connective tissue disease, abdominal aortic dissection, and mycotic or infectious abdominal aortic aneurysms; (2) documented coronary or structural heart disease, diabetes, severe renal or hepatic dysfunction, and cancer; and (3) a contraindication to computed tomographic angiography or known allergy to contrast media. During the same period, control subjects (1) matched in age, sex, and history of hypertension and smoking and (2) undergoing computed tomographic angiography to exclude AAA were recruited in the metabolomics study (Table S2). All subjects were in a fasting state, and blood samples were taken in the morning (6 AM to 8 AM). Plasma was stored in aliquots at −80°C until the day of analysis.

Animal Studies

All animal experiments were conducted in compliance with the National Institutes of Health Guidelines on the Care and Use of Laboratory Animals (National Institutes of Health Publication, 8th edition, 2011) and approved by the Animal Ethics Committee of Shanghai Jiao Tong University. Both male and female mice, 8 to 12 weeks old, were used in this study. AngII (angiotensin II)- or $CaPO_4$-induced AAA models were established as reported.[14] Global *Nr1d1* knockout (*Nr1d1*$^{-/-}$) mice on a C57BL/6J background were kindly provided by Dr Ueli Schibler (University of Geneva, Geneva, Switzerland).[15] Then, *Nr1d1*$^{-/-}$ mice were crossed with *ApoE*$^{-/-}$mice to establish *ApoE*$^{-/-}$/*Nr1d1*$^{-/-}$ mice. *ApoE*$^{-/-}$/*Nr1d1*$^{+/+}$ littermates were used as controls. Conditional VSMC-specific *Nr1d1* knockout mice (*Nr1d1*$^{flox/flox}$*Tagln-Cre*, *Nr1d1*$^{\Delta SMC}$), endothelial cell–specific *Nr1d1* knockout mice (*Nr1d1*$^{flox/flox}$*Tie2-Cre*, *Nr1d1*$^{\Delta EC}$), and myeloid cell–specific *Nr1d1* knockout mice (*Nr1d1*$^{flox/flox}$*Lysm-Cre*, *Nr1d1*$^{\Delta M\phi}$) were generated by breeding *Nr1d1*^{floxed} mice with *Tagln-Cre* [B6.Cg-Tg(Tagln-cre)1Her/J, #017491], *Tie2-Cre* [B6.Cg-Tg(Tek-cre)1Ywa/J, #008863], and *Lysm-Cre* [B6.129P2-*Lyz2*$^{tm1(cre)Ifo}$/J, #004781] mice from Jackson Laboratory, respectively. Then, *Nr1d1*$^{\Delta SMC}$, *Nr1d1*$^{\Delta EC}$, and *Nr1d1*$^{\Delta M\phi}$ mice were crossed with *ApoE*$^{-/-}$ mice to establish *ApoE*$^{-/-}$/*Nr1d1*$^{\Delta SMC}$, *ApoE*$^{-/-}$/*Nr1d1*$^{\Delta EC}$, and *ApoE*$^{-/-}$/*Nr1d1*$^{\Delta M\phi}$ mice, respectively. *ApoE*$^{-/-}$/*Nr1d1*$^{flox/flox}$ littermates were used as controls.

Statistical Analysis

Continuous data are presented as mean ± SEM, and categorical variables are shown as the number (percentage). The Shapiro-Wilk test was used to determine data distribution normality. For comparisons between 2 groups, the Levene test was used to determine the equality of variances. Comparisons were performed by the Student *t* test (equal variances) or unequal variance *t* test (unequal variances) for normally distributed variables or the Mann-Whitney *U* test for variables not normally distributed. For multiple comparisons (>2 groups), the Brown-Forsythe test was used to evaluate the homogeneity of variance. If the data passed the equal variance test, a 1-way ANOVA analysis was used followed by the Bonferroni post hoc test; otherwise, a Welch ANOVA test was performed followed by a post hoc analysis using the Tamhane T2 method.[16] Two-way ANOVA followed by Bonferroni post hoc analysis was used when >2 groups and variables were compared. Survival curves were assessed with the Kaplan-Meier method and compared by log-rank tests. Bivariate comparisons of categorical variables were performed with the chi-square test or the Fisher exact test. Statistical analysis was performed using SPSS software version 25.0 and GraphPad Prism 8. A value of $P<0.05$ was considered statistically significant.

An Expanded Methods section is available in the Supplemental Material, which includes detailed methods on the following: AngII- or $CaPO_4$-induced AAA models,[14] culture and treatment of primary cells (ie, mouse aortic smooth muscle cells [MASMCs],[17] mouse aortic endothelial cells,[18] and mouse bone marrow–derived macrophages[19]), in vivo multimodal imaging analysis, histological analysis,[20] in situ dihydroethidium staining,[21] in situ zymography staining,[22] terminal deoxynucleotidyl transferase dUTP nick-end labeling staining, MitoTracker Red CMXRos and JC-1 staining, detection of mitochondrial DNA (mtDNA) damage, measurement of oxygen consumption rate, NanoString nCounter assay,[23] RNA sequencing, chromatin immunoprecipitation, dual luciferase reporter assay, metabolomic profiling,[24] Western blot analysis, real-time quantitative polymerase chain reaction (RT-qPCR) (Table S4), coimmunoprecipitation, and ELISA.

RESULTS

NR1D1 Is Upregulated in Human and Murine Aortic SMCs From AAA Tissues

To date, 49 members of the NR superfamily have been documented;[25] however, the role of the majority of NRs in AAA is unknown. To examine which NRs may be involved in the pathogenesis of AAA and identify NR

ORIGINAL RESEARCH ARTICLE

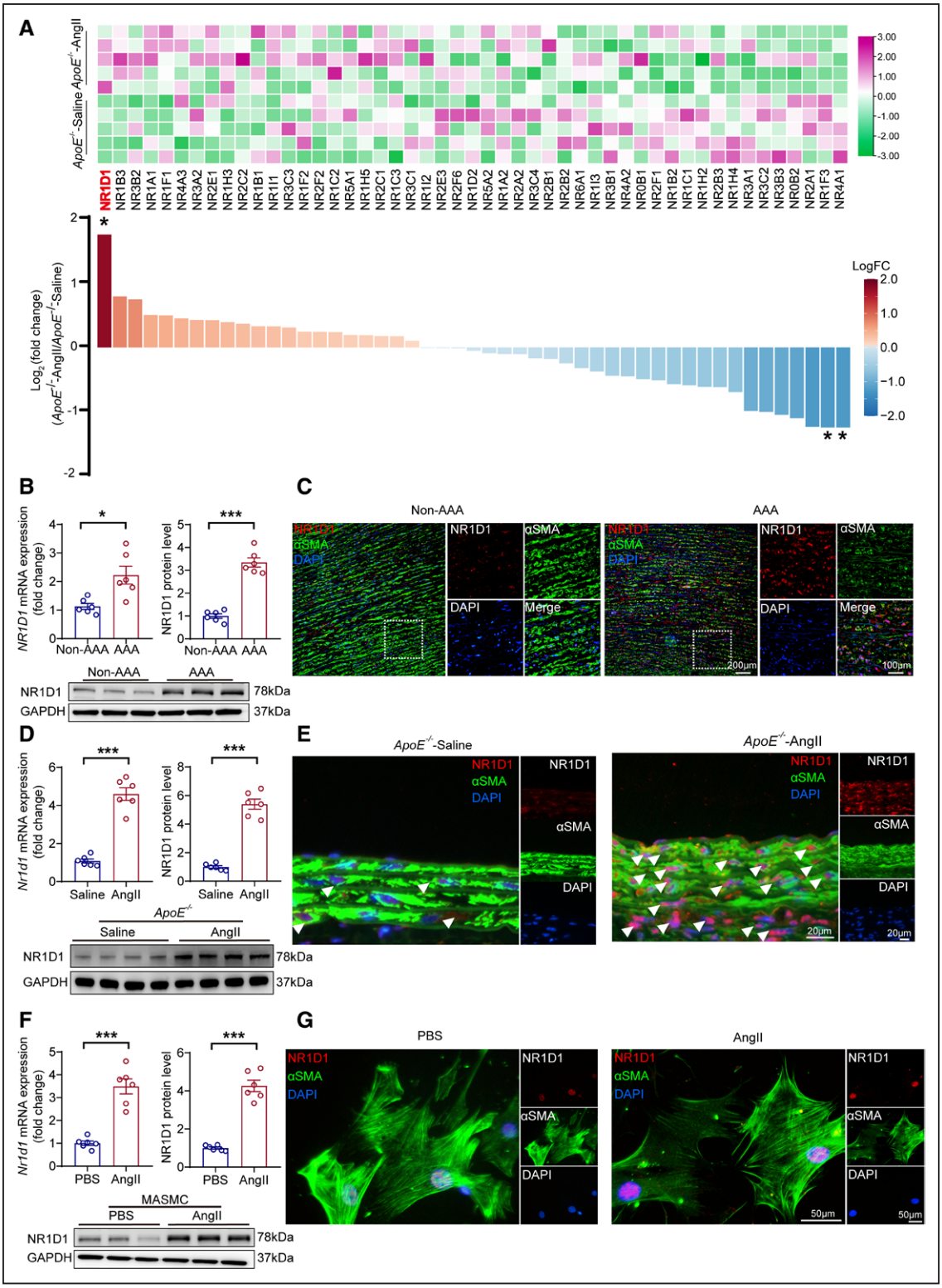

Figure 1. NR1D1 is upregulated in human and murine aortic SMCs from AAA tissues.

A, Relative mRNA expression of 49 NRs measured by Nanostring profiling in saline- or AngII-induced AAA mice (n=5 per group). The raw data were normalized to the mean expression levels of the housekeeping genes, and the normalized data were log2-transformed. The log2 (fold change) and *P* values were calculated, and multiple testing using the Benjamini-Hochberg method was applied to adjust the *P* values. With a Benjamini-Hochberg adjusted $P<0.05$ and $|\log2(\text{fold change})|\geq 1$ as the criteria, 3 genes (*Nr1d1* [adjusted $P=0.03$], *Nr4a1* [adjusted $P=0.04$], and *Nr1f3* [adjusted $P=0.04$]) were identified as differentially expressed NRs in mouse AAA tissues. *Benjamini–Hochberg adjusted $P<0.05$. **B**, **Top**, Quantification of *NR1D1* mRNA and NR1D1 protein expression measured by RT-qPCR and Western blot in human AAA and non-AAA segments (n=6 per group). Data were analyzed by unequal variance *t* test. (*Continued*)

Figure 1 Continued. *$P<0.05$; ***$P<0.001$. **Bottom**, NR1D1 protein expression assessed by Western blot in human AAA and non-AAA segments. **C**, Representative images of NR1D1 expression by immunofluorescence staining of human AAA and non-AAA segments and costaining with the key SMC-associated marker αSMA and DAPI. **D**, **Top**, Quantification of *Nr1d1* mRNA and NR1D1 protein expression measured by RT-qPCR and Western blot in mouse abdominal aortic segments (n=6 per group). Data were analyzed by Student *t* test. ***$P<0.001$. **Bottom**, NR1D1 protein expression assessed by Western blot in mouse abdominal aortic segments. **E**, Representative images of NR1D1 expression by immunofluorescence staining in mouse suprarenal abdominal aortas and costaining with αSMA and DAPI. **F**, **Top**, Quantification of *Nr1d1* mRNA and NR1D1 protein expression measured by RT-qPCR and Western blot in isolated MASMCs after stimulation with PBS or AngII for 48 hours (n=6 independent experiments). Data were analyzed by Student *t* test. ***$P<0.001$. **Bottom**, NR1D1 protein expression assessed by Western blot in isolated MASMCs after stimulation with PBS or AngII for 48 hours. **G**, Representative images of NR1D1 expression by immunofluorescence staining in MASMCs and costaining with αSMA and DAPI. Data are expressed as mean ± SEM. AAA indicates abdominal aortic aneurysm; AngII, angiotensin II; DAPI, 4'6-diamidino-2-phenylindole; αSMA, α-smooth muscle actin; MASMCs, mouse aortic smooth muscle cells; NR1D1, nuclear receptor subfamily 1 group D member 1; *Nr1f3*, nuclear receptor subfamily 1 group F member 3; *Nr4a1*, nuclear receptor subfamily 4 group A member 1 NRs, nuclear receptors; PBS, phosphate-buffered saline; RT-qPCR, real-time quantitative polymerase chain reaction; and SMC, smooth muscle cell.

genes altered during AAA, we first used high-throughput NanoString profiling[23] to interrogate the expression profiles of all NR genes in the AngII-induced AAA mouse aorta. NR1D1 was identified as the member with the highest fold change in expression among 49 NR superfamily members in murine AAA tissues (Figure 1A). The upregulation of both *Nr1d1* mRNA and NR1D1 protein was confirmed in human AAA tissues (Figure 1B and 1C) and murine AAA tissues (Figure 1D and 1E), as shown by RT-qPCR and Western blot. Time-course studies suggested that NR1D1 expression was significantly elevated as early as 3 days in AngII-induced AAA tissues (Figure S1). Moreover, both *Nr1d1* mRNA and NR1D1 protein levels were significantly increased in $CaPO_4$-induced AAA tissues (Figure S2A through S2C). It is important that in situ immunofluorescence staining showed that elevated NR1D1 protein was predominantly located in aortic smooth muscle cells from both human (Figure 1C) and murine (Figure 1E) AAA tissues. To further confirm the upregulation of NR1D1 in VSMCs, MASMCs were isolated and treated with AngII. As shown by RT-qPCR, Western blot, and immunofluorescence staining, both *Nr1d1* mRNA and NR1D1 protein levels were significantly increased in AngII-treated MASMCs (Figure 1F and 1G). Together, our data indicated that NR1D1 was upregulated in aortic smooth muscle cells in AAA. Recent studies indicated that the activities of some NRs could be regulated by a redox mechanism.[26,27] We further demonstrated that AngII induced NR1D1 upregulation in VSMCs in a reactive oxygen species–dependent manner (detailed in the Expanded Results and Figure S3).

VSMC-Specific NR1D1 Deficiency Represses AAA Formation In Vivo

To determine whether the upregulation of NR1D1 mediates AAA injury or acts as a self-defensive anti-AAA signal, we tested the effects of global *Nr1d1* knockout (*Nr1d1*$^{-/-}$), VSMC-specific *Nr1d1* knockout (*Nr1d1*$^{\Delta SMC}$), endothelial cell–specific *Nr1d1* knockout (*Nr1d1*$^{\Delta EC}$), and myeloid cell–specific *Nr1d1* knockout (*Nr1d1*$^{\Delta M\phi}$) on AAA formation (Figure S4). We found that global *Nr1d1* knockout and VSMC-specific *Nr1d1* knockout significantly ameliorated AAA formation (Figure S4), suggesting that NR1D1 acted as a positive regulator of AAA pathogenesis. However, we did not observe any significant effects of endothelial cell–specific *Nr1d1* knockout or myeloid cell–specific *Nr1d1* knockout on AAA formation (Figure S4). Thus, we focused on the role of VSMC-derived NR1D1 in AAA formation and development in the following experiments.

In an AngII-induced AAA model, AngII infusion was administered to homozygous *ApoE*$^{-/-}$/*Nr1d1*$^{\Delta SMC}$ mice and their littermate controls (*ApoE*$^{-/-}$/*Nr1d1*$^{flox/flox}$) for 28 days (Figure 2A), and blood pressure, heart rate, and plasma lipids were monitored. AngII increased systolic and diastolic blood pressure similarly in *ApoE*$^{-/-}$/*Nr1d1*$^{\Delta SMC}$ and *ApoE*$^{-/-}$/*Nr1d1*$^{flox/flox}$ mice, and no significant difference was observed in heart rate and plasma lipids between *ApoE*$^{-/-}$/*Nr1d1*$^{\Delta SMC}$ and *ApoE*$^{-/-}$/*Nr1d1*$^{flox/flox}$ mice (Table S3). However, both male (Figure 2B through 2F) and female (Figure S5A through S5C) *ApoE*$^{-/-}$/*Nr1d1*$^{\Delta SMC}$ mice exhibited significantly ameliorated AAA formation in the AngII-induced AAA model. Compared with those in *ApoE*$^{-/-}$/*Nr1d1*$^{flox/flox}$ mice, decreased maximal diameter of suprarenal abdominal aortas and total aortic weight/body weight were observed in *ApoE*$^{-/-}$/*Nr1d1*$^{\Delta SMC}$ mice (Figure 2G and 2H). Ameliorated AAA formation was further validated by in vivo multimodal imaging analysis, including micro-ultrasound imaging and magnetic resonance imaging (Figure 2I through 2K).

Morphologically, histological analysis results revealed that VSMC-specific *Nr1d1* knockout mitigated arterial wall thickening and reduced elastic fiber degradation and collagen deposition in AngII-administered mouse aortas (Figure S6). To evaluate the degradation of the extracellular matrix in the aortic wall, we determined the expression and activity of MMP-2 (matrix metalloproteinase-2). MMP-2 expression and MMP activity were substantially increased in AngII-induced *ApoE*$^{-/-}$/*Nr1d1*$^{flox/flox}$ mice, whereas enhanced MMP-2 expression and MMP activity were dramatically abolished in the aorta of AngII-infused *ApoE*$^{-/-}$/*Nr1d1*$^{\Delta SMC}$ mice (Figure S7). Moreover, NR1D1 deficiency suppressed the expression of inflammatory factors (ie, IL-6 [interleukin-6], TNF-α [tumor necrosis factor-α], and MCP-1 [monocyte chemoattractant protein-1]) in the abdominal aortas (Figure S8A through S8F).

ORIGINAL RESEARCH ARTICLE

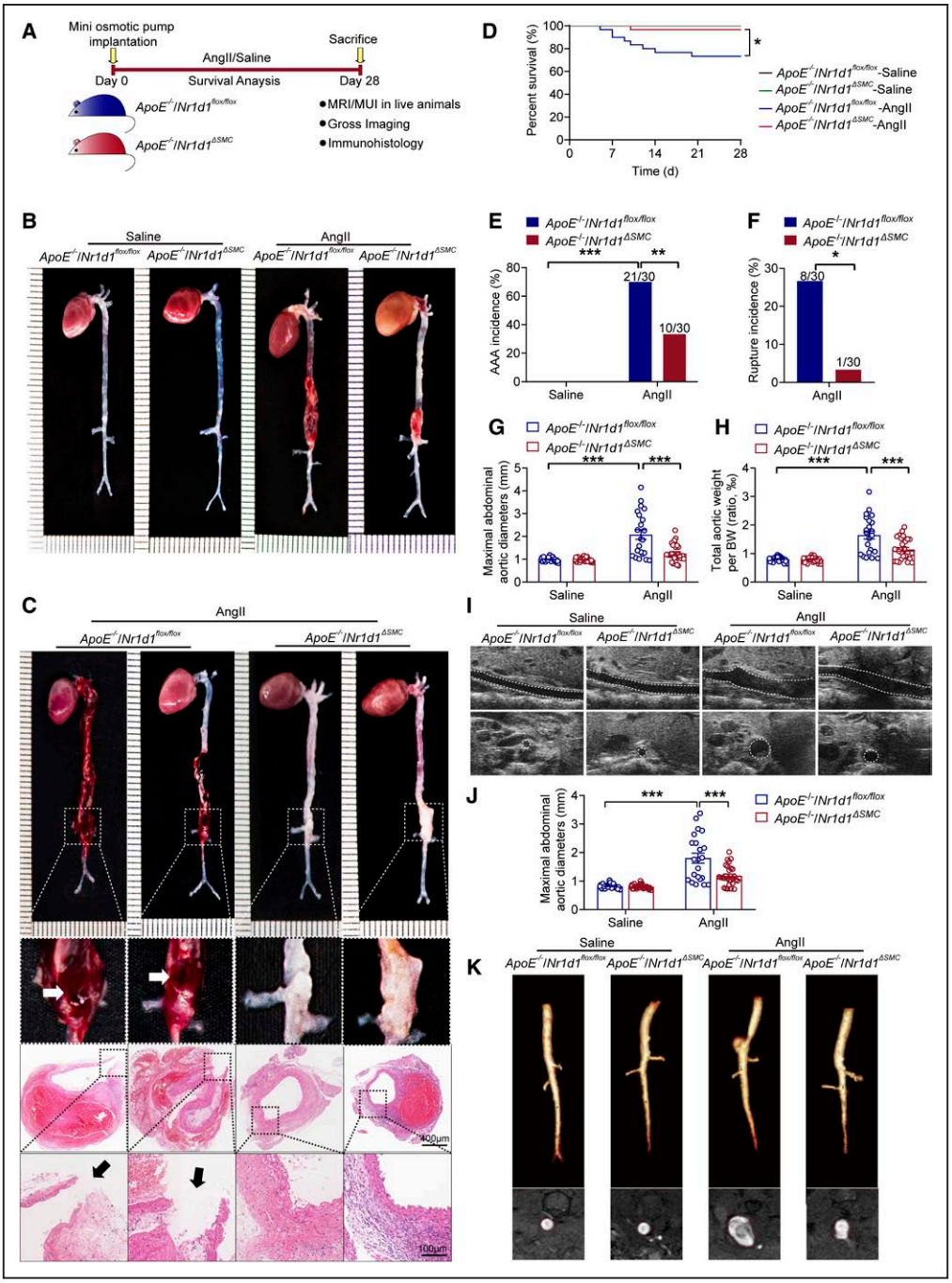

Figure 2. VSMC-specific NR1D1 deficiency represses AngII-induced AAA formation.
A, Schematic protocol: *ApoE*$^{-/-}$/*Nr1d1*$^{flox/flox}$ and *ApoE*$^{-/-}$/*Nr1d1*$^{\Delta SMC}$ mice were subcutaneously injected with saline or AngII by a mini osmotic pump for 28 days (n=30 per group). **B**, Representative images of the macroscopic features of AAA formation in indicated groups. **C**, Representative images of macroscopic features and HE staining of crossed-sections of aneurysm ruptures (arrow indicated). **D**, Survival curves in indicated groups (n=30 per group). Survival data were analyzed by the Kaplan-Meier method and compared using log-rank tests. **P*<0.05. **E**, The incidence of AngII-induced AAA in indicated groups (n=30 per group). Data were analyzed by a Fisher exact test. ***P*<0.01; ****P*<0.001. **F**, The incidence of AngII-induced aneurysm rupture in indicated groups (n=30 per group). Data were analyzed by a Fisher exact test. **P*<0.05. **G** and **H**, Quantification of the maximal diameter of suprarenal abdominal aortas measured by a Digital Vernier Caliper and total aortic weight/BW in indicated groups (n=22–30 per group). Data were analyzed by 2-way ANOVA followed by the Bonferroni post hoc test. ****P*<0.001. **I**, Representative images of abdominal aortas visualized by MUI using the B mode in indicated groups. **J**, Quantification of the maximal diameter of suprarenal abdominal aortas measured by MUI using the B mode in indicated groups (n=22–30 per group). Data were analyzed by 2-way ANOVA followed by the Bonferroni post hoc test. ****P*<0.001. **K**, Representative images of abdominal aortas visualized by MRI in indicated groups. **Top**, Abdominal aortas visualized using 3-dimensional time of flight fast low angle shot sequence (TOF-3D-Flash). **Bottom**, Abdominal aortas visualized by T2-weighted, PD-weighted imaging with multiple-echo multishot sequence (MEMS-PD-T2). Data are expressed as mean ± SEM. AAA indicates abdominal aortic aneurysm; AngII, angiotensin II; BW, body weight; EVG staining, elastin van Gieson staining; HE staining, hematoxylin and eosin staining; MUI, micro-ultrasound imaging; MRI, magnetic resonance imaging; NR1D1, nuclear receptor subfamily 1 group D member 1; and SMC, smooth muscle cell.

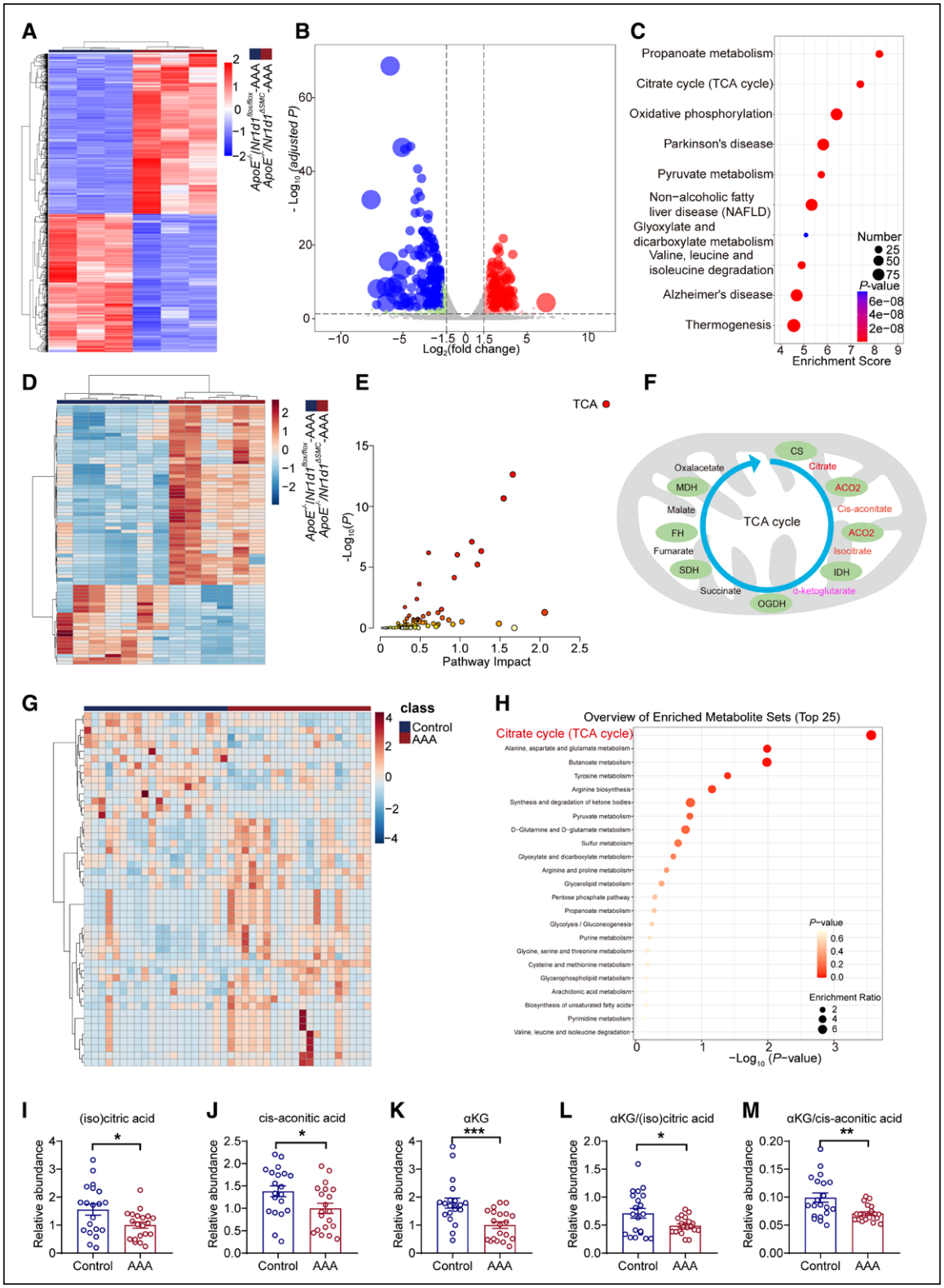

Figure 3. NR1D1 perturbs mitochondrial metabolism by the TCA cycle in AAA.
A, Heatmap of differentially expressed genes in *ApoE*$^{-/-}$/*Nr1d1*$^{flox/flox}$-AngII and *ApoE*$^{-/-}$/*Nr1d1*$^{\Delta SMC}$-AngII groups. Each column represents an individual replicate, and each row represents an individual gene. Upregulated genes are shown in red, and downregulated genes are displayed in blue. n=3 for both groups. Differentially expressed genes were defined as genes with a Benjamini-Hochberg adjusted *P* value <0.05 and |log2(fold change)|≥1. **B**, Volcano plot reveals the magnitude and significance of altered genes in *ApoE*$^{-/-}$/*Nr1d1*$^{flox/flox}$-AngII and *ApoE*$^{-/-}$/*Nr1d1*$^{\Delta SMC}$-AngII groups. Differentially expressed genes were defined as genes with a Benjamini-Hochberg adjusted *P* value <0.05 and |log2(fold change)|≥1. **C**, The top 10 Kyoto Encyclopedia Genes and Genomes (KEGG) pathways of differentially expressed genes. (*Continued*)

Figure 3 Continued. D, Heatmap of differential plasma metabolites in *ApoE*$^{-/-}$/*Nr1d1*$^{flox/flox}$-AngII and *ApoE*$^{-/-}$/*Nr1d1*$^{\Delta SMC}$-AngII groups. n=7 for *ApoE*$^{-/-}$/*Nr1d1*$^{flox/flox}$-AngII, n=6 for *ApoE*$^{-/-}$/*Nr1d1*$^{\Delta SMC}$-AngII. Differential metabolites in plasma were identified using variable important in projection (VIP) values of >1.2 in an orthogonal partial least squares–discriminant analysis (OPLS-DA) model. **E**, Multi-omics joint pathway analysis of transcriptomes and metabolomes. The highest ranked pathway is the TCA cycle. **F**, A combined analysis of transcriptome and metabolome profiles identified ACO2 in the TCA cycle as the potential target of NR1D1. The schematic illustration of intracellular metabolites and enzymes in the TCA metabolic pathway (modified from the combined analysis). CS, IDH, and OGDH are rate-limiting enzymes in the TCA cycle. **G**, Heatmap of differential plasma metabolites in patients with AAA and matched control subjects (n=20 per group). Differential metabolites in plasma were identified using VIP values of >1.2 in an OPLS-DA model. **H**, KEGG pathway enrichment analysis of human metabolomics. **I** through **M**, Relative abundances of (iso)citric acid, cis-aconitic acid, and αKG, and αKG to (iso)citrate/cis-aconitate ratios in patients with AAA and matched control subjects (n=20 per group). Data were analyzed by Student *t* test (**I**, **J**, and **L**) or Mann-Whitney *U* test (**K** and **M**). **P*<0.05; ***P*<0.01; ****P*<0.001. Data are expressed as mean ± SEM. AAA indicates abdominal aortic aneurysm; ACO2, aconitase-2; αKG, α-ketoglutarate; AngII, angiotensin II; CS, citrate synthase; FH, fumarate hydratase; IDH, isocitrate dehydrogenase; MDH, malate dehydrogenase; NR1D1, nuclear receptor subfamily 1 group D member 1; OGDH, oxoglutarate dehydrogenase; SDH, succinate dehydrogenase; and TCA, tricarboxylic acid.

To further confirm the pathogenic role of VSMC-derived NR1D1 in AAA formation, we performed experiments in another AAA model induced by $CaPO_4$. Compared with littermate *Nr1d1*$^{flox/flox}$ mice, *Nr1d1*$^{\Delta SMC}$ mice showed significantly ameliorated AAA formation and decreased maximal diameter of infrarenal abdominal aortas in the $CaPO_4$-induced AAA models in both male (Figure S2D through S2H) and female (Figure S5D through S5F) mice. *Nr1d1*$^{\Delta SMC}$ mice exhibited significantly decreased arterial wall thickness and reduced elastic fiber degradation and collagen deposition (Figure S9A through S9C) compared with littermate *Nr1d1*$^{flox/flox}$ controls. Furthermore, *Nr1d1*$^{\Delta SMC}$ mice displayed decreased MMP-2 expression and activity, and suppressed expression of inflammatory factors in the abdominal aorta compared with littermate *Nr1d1*$^{flox/flox}$ mice (Figure S9A, S9D, and S9F through S9H). Taken together, our data provided convincing evidence that VSMC-derived NR1D1 was a positive regulator that contributed to the pathogenesis of AAA.

NR1D1 Regulates Mitochondrial Metabolism by the TCA Cycle in AAA

To obtain deeper insight into the underlying mechanisms linking NR1D1 to the pathogenesis of AAA, high-throughput RNA-sequencing of mouse aortas was performed. Bioinformatics analyses of differentially expressed genes suggested that the upregulated genes were enriched in metabolism pathways (including propanoate metabolism, TCA cycle, and oxidative phosphorylation) (Figure 3A through 3C). Furthermore, metabolomic profiling was performed using plasma from AngII-infused *ApoE*$^{-/-}$/*Nr1d1*$^{\Delta SMC}$ mice and littermate *ApoE*$^{-/-}$/*Nr1d1*$^{flox/flox}$ mice by plasmonic nanoshells enhanced laser desorption/ionization mass spectrometry, and the top 75 differentially expressed metabolites were shown (Figure 3D). To screen the potential NR1D1 downstream candidates, we performed a combined analysis of transcriptomes (differentially expressed genes, Benjamini-Hochberg adjusted $P<0.05$ and $|\log2[\text{fold change}]|\geq1$) and metabolomes (metabolites, variable important in projection >1.2 using orthogonal partial least squares–discriminant analysis) with the MetaboAnalyst online tool (https://www.metaboanalyst.ca).[28] As shown in Figure 3E, the TCA cycle ranked as the top "core pathway" according to the joint pathway analysis. Collectively, the bioinformatics analyses implied that dysregulation of the mitochondrial TCA cycle caused by NR1D1 played a pivotal role in the pathogenesis of AAA. In addition, the joint pathway analysis suggested mitochondrial ACO2 as the downstream target for NR1D1 (Figure 3F). Because mitochondrial ACO2 dysfunction may result in decreased abundances of (iso)citrate, cis-aconitate, and αKG and reduced ratios of αKG to (iso)citrate/cis-aconitate, an indicator of TCA cycle breakdown,[29] we further examined the downstream signaling of ACO2. As expected, NR1D1 deficiency increased the abundances of isocitrate, cis-aconitate, and αKG, and the ratios of αKG to isocitrate/cis-aconitate (Figure S10). To consolidate these findings in humans, metabolomic profiling was performed in patients with AAA and matched controls. In agreement with the animal findings, differentially expressed metabolites and enrichment analysis demonstrated that the TCA cycle was the top-ranked core pathway (Figure 3G and 3H). The abundances of (iso)citrate, cis-aconitate, and αKG, the downstream metabolites of ACO2, were downregulated in human AAA plasma samples (Figure 3I through 3K). Moreover, patients with AAA had significantly lower αKG to (iso)citrate/cis-aconitate ratios (Figure 3L and 3M).

Aco2 Is the Direct Trans-Repression Target of NR1D1 in Regulating Mitochondrial Metabolism

We further examined the expression and activity of the key TCA cycle enzyme ACO2 in both human and mouse AAA samples. Compared with those in non-AAA sections, ACO2 expression and activity were dramatically decreased in human AAA sections (Figure 4A through 4D). Consistent with these results in human AAA tissues, the expression and activity of ACO2 were reduced in AngII-treated AAA mouse aortas (Figure 4E through 4H; Figure S11). To further validate that mitochondrial ACO2 was the nodal point involved in the pathogenesis of AAA regulated by NR1D1, we examined the effect of *Nr1d1*$^{\Delta SMC}$

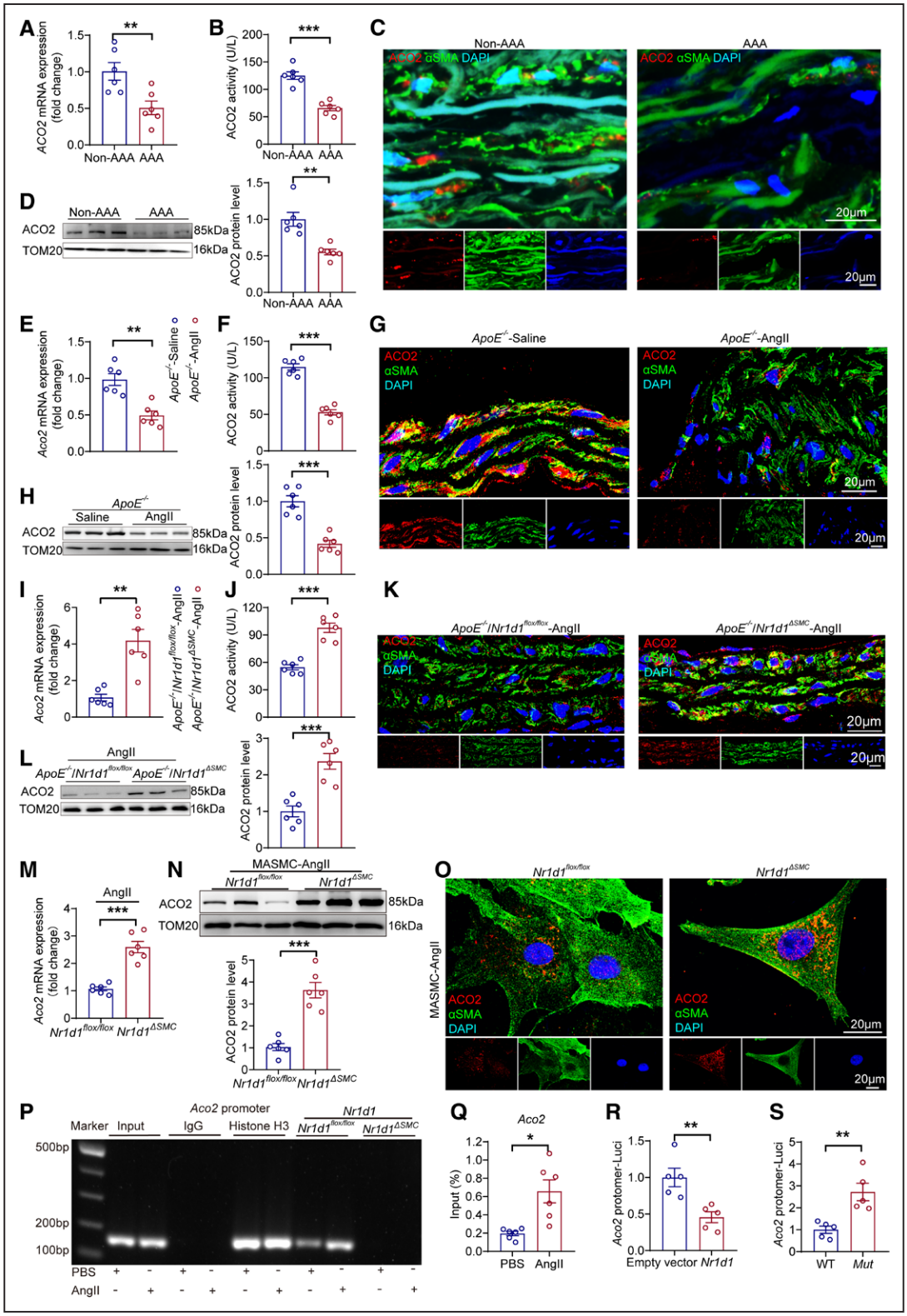

Figure 4. *Aco2* is the direct trans-repression target of NR1D1 in regulating mitochondrial function.
A and **B**, *Aco2* mRNA expression and ACO2 activity measured by RT-qPCR and ELISAs in human AAA and non-AAA segments (n=6 per group). Data were analyzed by Student *t* test. $^{**}P<0.01$; $^{***}P<0.001$. **C**, Representative images of ACO2 expression by immunofluorescence staining of human AAA and non-AAA segments and costaining with the key smooth muscle cell–associated marker αSMA and DAPI. **D**, **Left**, ACO2 protein expression assessed by Western blot in human AAA and non-AAA segments. **Right**, Quantification of ACO2 protein expression measured by Western blot in indicated groups (n=6 per group). Data were analyzed by Student *t* test. $^{**}P<0.01$. **E** and **F**, *Aco2* mRNA expression and ACO2 activity measured by RT-qPCR and ELISAs in abdominal aortic segments from saline- and AngII-infused *ApoE*$^{-/-}$ mice (n=6 per group). (*Continued*)

Figure 4 Continued. Data were analyzed by Student *t* test. ***P*<0.01; ****P*<0.001. **G**, Representative images of ACO2 expression by immunofluorescence staining in abdominal aortas from saline- and AngII-infused *ApoE*$^{-/-}$ mice. **H**, **Left**, ACO2 protein expression measured by Western blot in abdominal aortas from saline- and AngII-infused *ApoE*$^{-/-}$ mice. **Right**, Quantification of ACO2 protein expression measured by Western blot in indicated groups (n=6 per group). Data were analyzed by Student *t* test. ****P*<0.001. **I** and **J**, *Aco2* mRNA expression and ACO2 activity measured by RT-qPCR and ELISAs in abdominal aortas from AngII-infused *ApoE*$^{-/-}$/*Nr1d1*$^{flox/flox}$ and *ApoE*$^{-/-}$/*Nr1d1*$^{\Delta SMC}$ mice (n=6 per group). Data were analyzed by Student *t* test. ***P*<0.01; ****P*<0.001. **K**, Representative images of ACO2 expression by immunofluorescence staining in abdominal aortas from AngII-infused *ApoE*$^{-/-}$/*Nr1d1*$^{flox/flox}$ and *ApoE*$^{-/-}$/*Nr1d1*$^{\Delta SMC}$ mice. **L**, **Left**, ACO2 protein expression measured by Western blot in abdominal aortas from AngII-infused *ApoE*$^{-/-}$/*Nr1d1*$^{flox/flox}$ and *ApoE*$^{-/-}$/*Nr1d1*$^{\Delta SMC}$ mice. **Right**, Quantification of ACO2 protein expression measured by Western blot in indicated groups (n=6 per group). Data were analyzed by Student *t* test. ****P*<0.001. **M**, *Aco2* mRNA expression measured by RT-qPCR in MASMCs isolated from *Nr1d1*$^{flox/flox}$ and *Nr1d1*$^{\Delta SMC}$ mice after stimulation with AngII for 48 h (n=6 independent experiments). Data were analyzed by Student *t* test. ****P*<0.001. **N**, **Top**, Mitochondrial ACO2 protein expression measured by Western blot in MASMCs isolated from *Nr1d1*$^{flox/flox}$ and *Nr1d1*$^{\Delta SMC}$ mice after stimulation with AngII for 48 hours. **Bottom**, Quantification of ACO2 protein expression measured by Western blot in indicated groups (n=6 independent experiments). Data were analyzed by Student *t* test. ****P*<0.001. **O**, Representative images of ACO2 expression by immunofluorescence staining in MASMCs isolated from *Nr1d1*$^{flox/flox}$ and *Nr1d1*$^{\Delta SMC}$ mice after stimulation with AngII for 48 hours. **P**, ChIP-qPCR was performed with antibodies to NR1D1, and the target promoter region of *Aco2* was amplified by qPCR. **Q**, Quantification of ChIP-qPCR (n=6 independent experiments). Data were analyzed by Student *t* test. **P*<0.05. **R**, MASMCs were cotransfected with empty or *Nr1d1* plasmid and pGL3-*Aco2*-promoter-Luci plasmid for 48 hours (n=5 independent experiments). Data were analyzed by Student *t* test. ***P*<0.01. **S**, MASMCs were cotransfected with *Nr1d1* plasmid and pGL3-m_wt*Aco2*-promoter-Luci (WT) or pGL3-m_mut*Aco2*-promoter-Luci plasmid (*Mut*) for 48 hours (n=5 independent experiments). Data were analyzed by Student *t* test. ***P*<0.01. Data are expressed as mean ± SEM. AAA indicates abdominal aortic aneurysm; ACO2, aconitase-2; AngII, angiotensin II; ChIP, chromatin immunoprecipitation; MASMCs, mouse aortic smooth muscle cells; NR1D1, nuclear receptor subfamily 1 group D member 1; RT-qPCR, real-time quantitative polymerase chain reaction; and WT, wild type.

on mitochondrial ACO2 expression and activity in mouse aortas after AngII treatment. The mRNA and protein expression levels and enzymatic activity of mitochondrial ACO2 were significantly elevated in *ApoE*$^{-/-}$/*Nr1d1*$^{\Delta SMC}$ AAA mice compared with those in *ApoE*$^{-/-}$/*Nr1d1*$^{flox/flox}$ AAA mice (Figure 4I through 4L). Furthermore, mitochondrial ACO2 expression was upregulated in AngII-treated MASMCs isolated from *Nr1d1*$^{\Delta SMC}$mice compared with that from *Nr1d1*$^{flox/flox}$ mice (Figure 4M through 4O).

NR1D1 functions as a transcriptional repressor by recruiting NCoR1 (nuclear receptor corepressor 1) and HDAC3 (histone deacetylase 3).[30] As expected, coimmunoprecipitation and immunoblotting experiments indicated that Ad*Nr1d1* transfection-mediated overexpression of NR1D1 enhanced the interaction between NCoR1-HDAC3 and NR1D1 (Figure S12A and S12B). Consistently, enhanced interactions between NR1D1 and NCoR1-HDAC3 complexes were observed in MASMCs treated with AngII compared with those in MASMCs treated with saline (Figure S12C). The putative binding site of mouse NR1D1 (through its recruitment of NCoR1) in the promoter region of the mouse *Aco2* locus (*GCCCCAC*, -65 bp to -58 bp) was predicted by the Catalog of Inferred Sequence Binding Preferences (CIS-BP) database (http://cisbp.ccbr.utoronto.ca), which was confirmed by chromatin immunoprecipitation–polymerase chain reaction (Figure 4P enrolled patients with both thoracic and 4Q; Figure S12D). Moreover, dual luciferase reporter assays showed that NR1D1 overexpression repressed *Aco2* promoter activity (*Aco2-wt*, -2000 to +98 bp) (Figure 4R), and mutant promoter activity (*Aco2-mut*) was higher than *Aco2*-wt promoter activity in MASMCs (Figure 4S). Taken together, these data identified ACO2 as the direct trans-repression target of NR1D1 in regulating mitochondrial metabolism.

Protective Role of NR1D1 Deficiency in Mitochondrial Function Is Mediated by ACO2

TCA cycle metabolites contribute to the maintenance of mitochondrial homeostasis, and alterations in mitochondrial metabolism can lead to impaired mitochondrial respiration, mtDNA damage, and electron transport chain (ETC) defects.[31] Thus, we further investigated the effect of *Nr1d1* deficiency on mitochondrial function in AAA development. Oxygen consumption analysis revealed significantly increased basal, maximal, and ATP-coupled mitochondrial oxygen consumption rates in AngII-treated MASMCs isolated from *Nr1d1*$^{\Delta SMC}$ mice compared with those in MASMCs from *Nr1d1*$^{flox/flox}$ littermates (Figure 5A through 5D). Moreover, *Nr1d1* deficiency decreased AngII-induced mtDNA damages in cultured MASMCs isolated from *Nr1d1*$^{\Delta SMC}$ mice compared with those in MASMCs from *Nr1d1*$^{flox/flox}$ mice (Figure 5E). Furthermore, RT-qPCR results showed an increase in nuclear-encoded mitochondrial genes and mtDNA-encoded genes of ETC complexes in *Nr1d1*$^{\Delta SMC}$-MASMCs compared with those in *Nr1d1*$^{flox/flox}$-MASMCs after AngII treatment (Figure 5F and 5G). In addition, RNA-sequencing data validated that *Nr1d1* deficiency significantly upregulated the RNA levels of nuclear-encoded mitochondrial genes and mtDNA-encoded genes of ETC complexes (Figure 5H and 5I), and the results were further confirmed by RT-qPCR and Western blot (Figure 5J through 5L). Moreover, in situ dihydroethidium staining and terminal deoxynucleotidyl transferase dUTP nick-end labeling assays indicated significantly reduced mitochondrial apoptosis and reactive oxygen species production in *ApoE*$^{-/-}$/*Nr1d1*$^{\Delta SMC}$ mouse aortas (Figure 5M and 5N; Figure S8G through S8I). Consistent results were observed in *Nr1d1*$^{\Delta SMC}$ mice after $CaPO_4$ treatment (Figure S9A, S9D, and S9E). Collectively, these data indicated that NR1D1 regulated mitochondrial homeostasis in AAA.

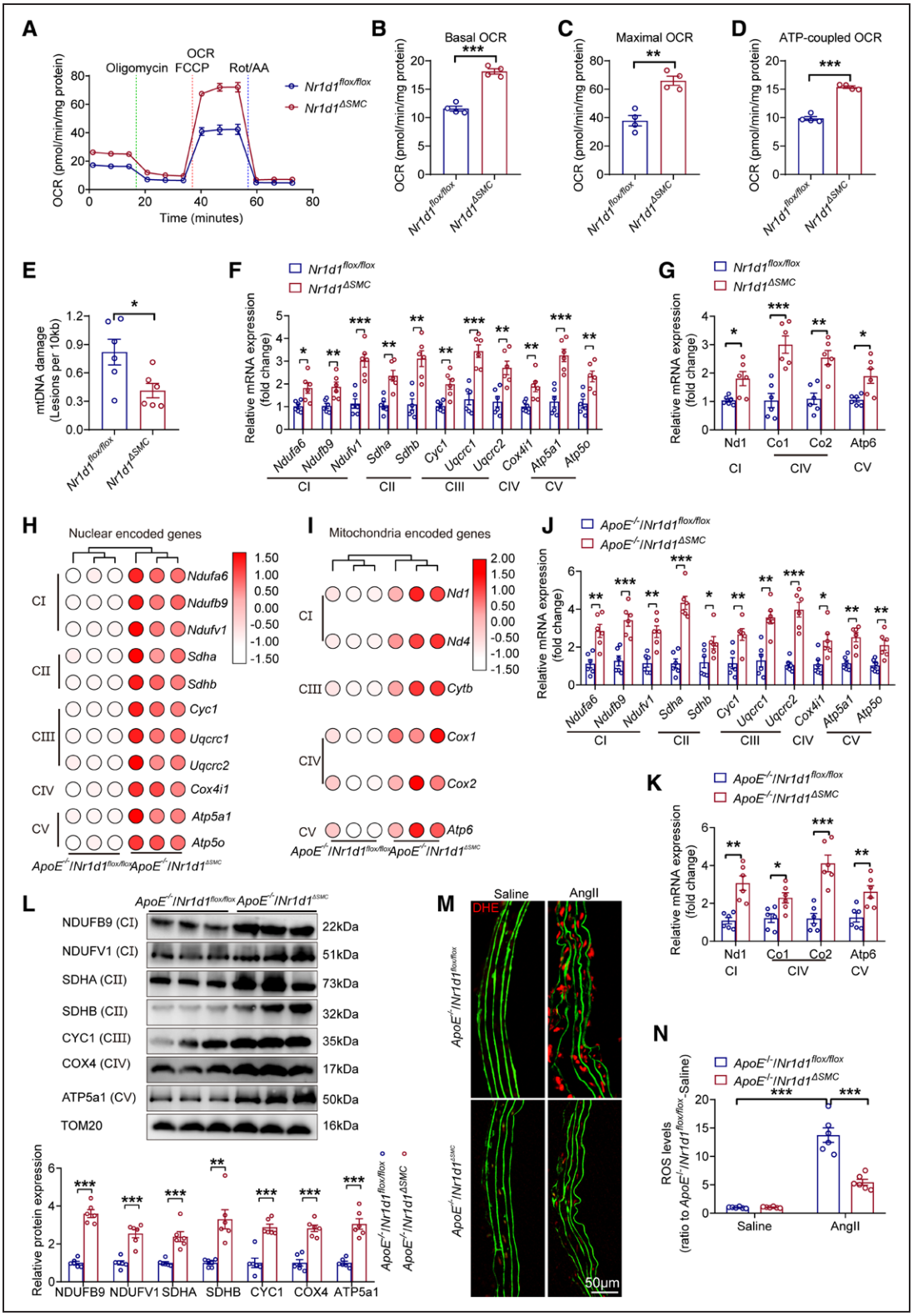

Figure 5. VSMC-specific NR1D1 deficiency regulates the expression of mitochondria-related genes and inhibits mitochondrial ROS production.

A, Summarized OCR tracings in MASMCs isolated from *Nr1d1*$^{flox/flox}$ and *Nr1d1*$^{\Delta SMC}$ mice after stimulation with AngII for 48 hours (n=4 independent experiments). **B** through **D**, Basal, maximal, and ATP-coupled OCRs in indicated groups (n=4 independent experiments). Data were analyzed by Student *t* test. $^{**}P<0.01$; $^{***}P<0.001$. **E**, mtDNA damage detection in MASMCs isolated from *Nr1d1*$^{flox/flox}$ and *Nr1d1*$^{\Delta SMC}$ mice after stimulation with AngII for 48 hours (n=6 independent experiments). Data were analyzed by Student *t* test. $^{*}P<0.05$. **F** and **G**, Relative mRNA expression of nuclear- and mitochondrial-encoded mitochondrial genes in MASMCs isolated from *Nr1d1*$^{flox/flox}$ and *Nr1d1*$^{\Delta SMC}$ mice with AngII treatment for 48 hours, normalized to *β-actin* (n=6 independent experiments). Data were analyzed by Student *t* test. (*Continued*)

Figure 5 Continued. *P<0.05; **P<0.01; ***P<0.001. **H** and **I**, Heatmap of log2 (fold change) of nuclear- and mitochondrial-encoded mitochondrial genes in the abdominal aorta from AngII-infused *ApoE*$^{-/-}$/*Nr1d1*$^{flox/flox}$ and *ApoE*$^{-/-}$/*Nr1d1*$^{\Delta SMC}$ mice (n=3 per group). Differentially expressed genes were defined as genes with a Benjamini-Hochberg adjusted P value <0.05 and |log2(fold change)| ≥1. **J** and **K**, Relative mRNA expression of nuclear and mitochondria-encoded mitochondrial genes in AngII-infused *ApoE*$^{-/-}$/*Nr1d1*$^{flox/flox}$ and *ApoE*$^{-/-}$/*Nr1d1*$^{\Delta SMC}$ mice (n=6 per group). Data were analyzed by Student t test. *P<0.05; **P<0.01; ***P<0.001. **L**, **Top**, Protein expression of mitochondrial complexes in abdominal aortas from AngII-infused *ApoE*$^{-/-}$/*Nr1d1*$^{flox/flox}$ and *ApoE*$^{-/-}$/*Nr1d1*$^{\Delta SMC}$ mice. **Bottom**, Quantification of protein expression of mitochondrial complexes in indicated groups (n=6 per group). Data were analyzed by Student t test. *P<0.05; ***P<0.001. **M** and **N**, Representative images of in situ DHE staining and quantification of ROS levels in suprarenal abdominal aortas to assess superoxide generation in indicated groups (n=6 per group). Data were analyzed by 2o-way ANOVA followed by the Bonferroni post hoc test. ***P<0.001. Data are expressed as mean ± SEM. AngII indicates angiotensin II; DHE, dihydroethidium; MASMCs, mouse aortic smooth muscle cells; mtDNA, mitochondrial DNA; NR1D1, nuclear receptor subfamily 1 group D member 1; OCR, oxygen consumption rate; ROS, reactive oxygen species; and SMC, smooth muscle cell.

To determine whether these findings were direct effects of NR1D1 deletion or the consequence of AAA inhibition, abdominal aortas from *ApoE*$^{-/-}$/*Nr1d1*$^{flox/flox}$ and *ApoE*$^{-/-}$/*Nr1d1*$^{\Delta SMC}$ mice were harvested on the morning of day 3 after AngII infusion before a change in AAAs. NR1D1 deficiency restored the ACO2 dysregulation and mitochondrial dysfunction, as well as inhibited reactive oxygen species levels and inflammatory markers before a change in AAAs on day 3 after AngII infusion (Figure 6).

To further study whether the protective effects of *Nr1d1* deficiency on mitochondrial function were mediated by ACO2, a small-interfering RNA targeting *Aco2* mRNA (si*Aco2*) was transfected into cultured MASMCs (Figure 7A). ACO2 silencing reduced basal, maximal, and ATP-coupled oxygen consumption rates (Figure 7B; Figure S13), exacerbated AngII-induced mtDNA damage (Figure 7C), and reversed the protective effects of *Nr1d1* knockout in MASMCs (Figure 7B and 7C; Figure S13). Furthermore, *Nr1d1* deficiency reversed the decrease in mitochondrial membrane potential ($\Delta\Psi m$), mitochondrial apoptosis, and mitochondrial ETC complexes, and inhibited extracellular matrix degradation (MMP-2 expression and activity) in MASMCs after AngII treatment (Figure 7D through 7I). It is important that these protective effects could be nullified by *Aco2* knockdown (Figure 7B through 7I; Figure S13). Taken together, these data suggested that the protective role of *Nr1d1* deficiency against mitochondrial dysfunction was mediated by ACO2.

Supplementation With the ACO2 Downstream Metabolite αKG Protects Against AAA Formation

In the TCA cycle, ACO2 catalyzes the reversible transformation of citrate to isocitrate, and isocitrate dehydrogenase triggers the conversion of isocitrate to αKG (a rate-limiting step of the TCA cycle) (Figure 3F).[31] Thus, we wondered whether the impaired TCA cycle in AAAs would be reactivated by supplementing the key metabolic downstream product αKG. To verify this hypothesis, saline- or AngII-infused *ApoE*$^{-/-}$/*Nr1d1*$^{flox/flox}$ and *ApoE*$^{-/-}$/*Nr1d1*$^{\Delta SMC}$ mice were intraperitoneally administered vehicle or DM-αKG (dimethyl α-ketoglutarate) daily for 4 weeks[32] (Figure 8A). DM-αKG supplementation reduced AngII-induced AAAs in *ApoE*$^{-/-}$/*Nr1d1*$^{flox/flox}$ mice, as evidenced by the significant difference in AAA formation in DM-αKG– or saline-treated *ApoE*$^{-/-}$/*Nr1d1*$^{flox/flox}$ mice (Figure 8B through 8G). Moreover, DM-αKG supplementation significantly reduced pathological collagen deposition, elastin degradation, and extracellular matrix degradation (MMP-2 expression and activity) and increased mitochondrial ETC complex expression in AngII-induced AAA tissues (Figure S14). Moreover, αKG supplementation attenuated aneurysm progression in a preestablished AAA mouse model[33] (detailed in the Expanded Results and Figure S15). The vasoprotective effects of DM-αKG supplementation against AAA formation were further validated in the $CaPO_4$-induced AAA model (Figure S16). Consistently, in vitro experiments showed that the addition of DM-αKG[32] significantly reversed AngII-induced injuries in MASMCs (Figure S17). These data provided convincing evidence that supplementation with the ACO2 downstream metabolite αKG protected against AAA injuries.

In the next series of experiments, MASMCs were transfected with AdCon or Ad*Nr1d1* for 48 hours and treated with AngII. NR1D1 overexpression in MASMCs decreased mitochondrial respiratory capacity, mitochondrial membrane potential, and mitochondrial ETC complexes, and promoted mitochondrial apoptosis and extracellular matrix degradation after AngII treatment (Figure S18). However, DM-αKG treatment reversed the detrimental effects of NR1D1 overexpression on mitochondrial respiratory capacity, mitochondrial membrane potential, mitochondrial ETC complexes, mitochondrial apoptosis, and extracellular matrix degradation (Figure S18). These results suggested that αKG supplementation nullified the detrimental effect of NR1D1 on mitochondrial function.

DISCUSSION

In the present work, we identified a novel role of the nuclear receptor NR1D1 in the pathogenesis of AAA. The novel contributions included the following. First, we identified that *Nr1d1* gene expression exhibited the highest fold change among all 49 NRs in AAA tissues, and NR1D1 protein was upregulated in both human and

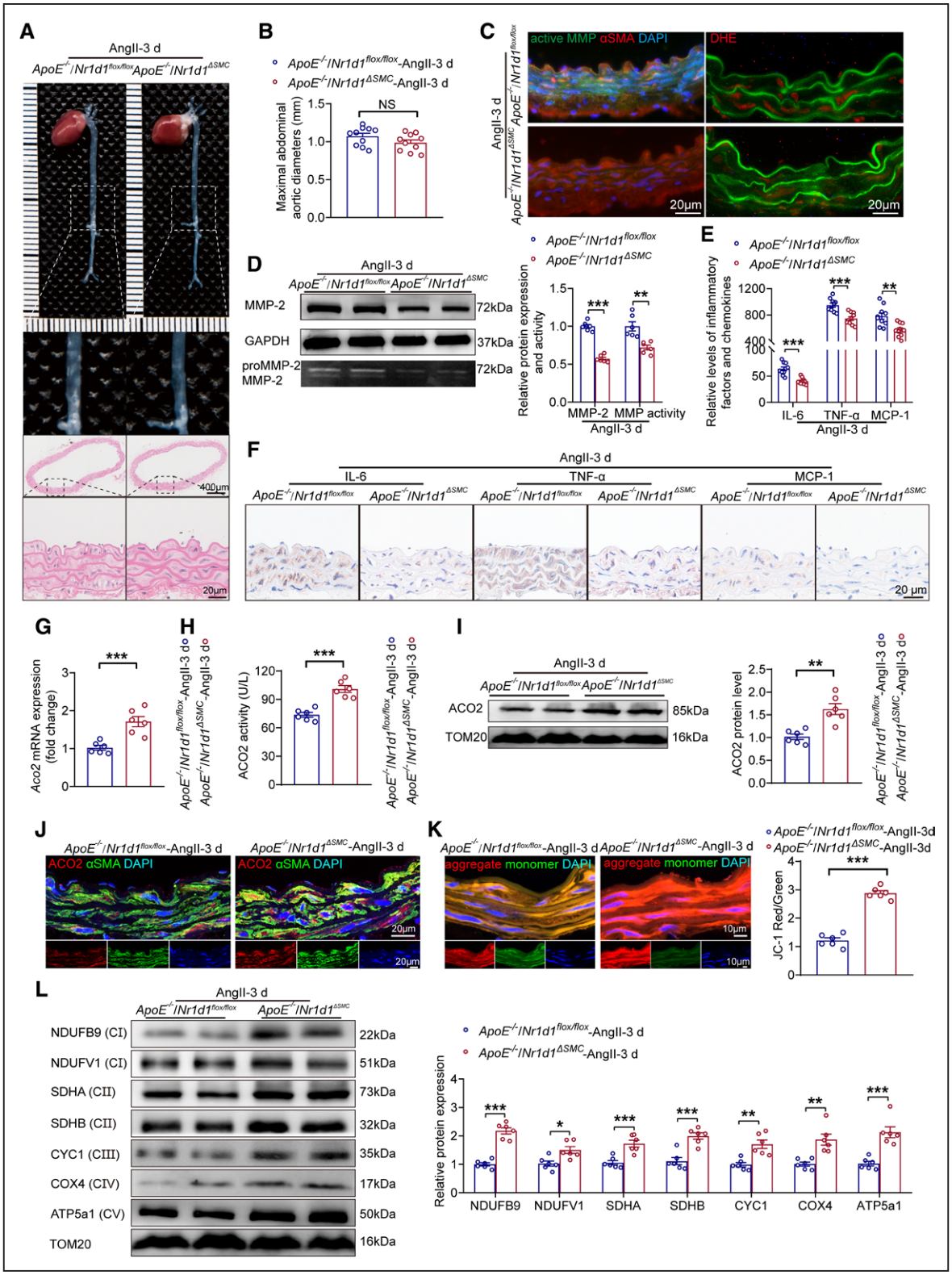

Figure 6. NR1D1 deficiency results in early changes in mitochondrial function on day 3 after AngII infusion before a change in AAAs.

Abdominal aortas from *ApoE*$^{-/-}$/*Nr1d1*$^{flox/flox}$ and *ApoE*$^{-/-}$/*Nr1d1*$^{\Delta SMC}$ mice were harvested on the morning of day 3 after AngII infusion before a change in AAAs. **A**, Representative images of the macroscopic features and HE staining of suprarenal abdominal aortas in *ApoE*$^{-/-}$/*Nr1d1*$^{flox/flox}$ and *ApoE*$^{-/-}$/*Nr1d1*$^{\Delta SMC}$ mice on day 3 after AngII infusion. **B**, Quantification of the maximal diameter of suprarenal abdominal aortas in indicated groups (n=10 per group). Data were analyzed by Student *t* test. **C**, Representative images of MMP activity and in situ DHE staining in indicated groups. **D**, **Left**, MMP-2 protein expression measured by Western blot and MMP activity measured by zymography in indicated groups. **Right**, Quantification of MMP-2 protein expression and MMP activity in indicated groups (n=6 per group). (*Continued*)

Figure 6 Continued. Data were analyzed by Student *t* test. ***P*<0.01; ****P*<0.001. **E**, IL-6, TNF-α, and MCP-1 expression in abdominal aortas assessed by ELISAs in indicated groups (n=10 per group). Data were analyzed by Student *t* test. ***P*<0.01; ****P*<0.001. **F**, IL-6, TNF-α, and MCP-1 expression measured by immunohistochemistry in indicated groups. **G** and **H**, *Aco2* mRNA expression and ACO2 activity measured by RT-qPCR and ELISAs in abdominal aortas from *ApoE*$^{-/-}$/*Nr1d1*$^{flox/flox}$ and *ApoE*$^{-/-}$/*Nr1d1*$^{\Delta SMC}$ mice on day 3 after AngII infusion (n=6 per group). Data were analyzed by Student *t* test. ****P*<0.001. **I**, **Left**, ACO2 protein expression measured by Western blot in abdominal aortas from *ApoE*$^{-/-}$/*Nr1d1*$^{flox/flox}$ and *ApoE*$^{-/-}$/*Nr1d1*$^{\Delta SMC}$ mice on day 3 after AngII infusion. **Right**, Quantification of ACO2 protein expression measured by Western blot in indicated groups (n=6 per group). Data were analyzed by Student *t* test. ***P*<0.01. **J**, Representative images of ACO2 expression by immunofluorescence staining in indicated groups. **K**, **Left**, Representative images of mitochondrial ΔΨm by JC-1 staining in indicated groups. **Right**, Quantification of JC-1 staining (n=6 per group). Data were analyzed by Student *t* test. ****P*<0.001. **L**, **Left**, Protein expression of mitochondrial complexes in the abdominal aortas from AngII-infused *ApoE*$^{-/-}$/*Nr1d1*$^{flox/flox}$ and *ApoE*$^{-/-}$/*Nr1d1*$^{\Delta SMC}$ mice on day 3 after AngII infusion. **Right**, Quantification of protein expression of mitochondrial complexes in indicated groups (n=6 per group). Data were analyzed by Student *t* test. **P*<0.05; ***P*<0.01; ****P*<0.001. Data are expressed as mean ± SEM. ACO2 indicates aconitase-2; AngII, angiotensin II; DHE, dihydroethidium; IL-6, interleukin-6; MCP-1, monocyte chemoattractant protein-1; MMP, matrix metalloproteinase; NR1D1, nuclear receptor subfamily 1 group D member 1; NS, nonsignificant; RT-qPCR, real-time quantitative polymerase chain reaction; SMC, smooth muscle cell; and TNF-α, tumor necrosis factor-α.

MASMCs from AAA tissues. Moreover, global and VSMC-specific knockout of *Nr1d1* protected mice against AAA formation in both AngII- and $CaPO_4$-induced AAA models. Furthermore, mechanistic studies identified ACO2, a key enzyme of the mitochondrial TCA cycle, as a direct transcriptional downstream target trans-repressed by NR1D1 that mediated the negative effects of NR1D1 on mitochondrial function and AAA formation. Last, supplementation with αKG, a downstream metabolic product of ACO2, was sufficient to protect against AAA formation and abolish the detrimental effect of NR1D1 overexpression on mitochondrial function (Figure 8H). Collectively, the results of the present study provided the first evidence for a novel regulatory NR1D1-ACO2-αKG signaling axis in AAA formation and progression.

As transcription factors, NRs regulate gene expression not only during physiological processes (metabolic and immunology response programs) but also during several pathological conditions, including cancer, metabolic disorders, and cardiovascular diseases.[25,34] NR1D1 is a special member of the metabolic NR superfamily known as a core regulator of circadian rhythms.[35,36] In addition to its classical functions in controlling circadian rhythms, recent studies have uncovered several new functions of NR1D1 (ie, regulating cell metabolism and inflammatory responses) in the pathogenesis of metabolic disease, cancer, and muscular dysfunction.[37,38] It is important that emerging evidence has shown that NR1D1 regulates cardiovascular physiology/pathology.[8,9,13] Although NR1D1 has been reported to inhibit atherosclerotic development,[13] we unexpectedly found a profound detrimental effect of NR1D1 on AAA development. NR1D1 was upregulated in human and MASMCs from AAA tissues, with its gene expression ranked the highest in fold change among all 49 NRs. VSMC-specific *Nr1d1* knockout significantly ameliorated AAA formation in 2 different animal models. The detrimental effect of NR1D1 was further confirmed by in vitro MASMC experiments. These data provided convincing evidence of a previously unrecognized role of VSMC-derived NR1D1 as a positive regulator contributing to the pathogenesis of AAA. In the present study, global *Nr1d1* knockout and VSMC-specific *Nr1d1* knockout (but not endothelial cell–specific *Nr1d1* knockout or macrophage-specific *Nr1d1* knockout) significantly inhibited AAA formation, suggesting a cell-specific role of NR1D1 in different vascular diseases.

NR1D1 has been shown to control glucose and lipid metabolism tightly in several organs and cells.[35,39] In the present study, through integrated transcriptomic, metabolomic, and epigenomic profiling analyses, the key mitochondrial TCA cycle enzyme ACO2 was identified as a direct transcriptional downstream target trans-repressed by NR1D1 and found to mediate the detrimental effects of NR1D1 on mitochondrial metabolism. The TCA cycle, also known as the citric acid cycle or the Krebs cycle, is a series of reactions in a closed loop that forms a metabolic engine to control cell function and cell fate by regulating the generation of ATP and metabolites.[31] Aberrant TCA cycle function is implicated in a wide variety of pathological conditions, such as cancer and diabetes.[40,41] The enzyme ACO2 is indispensable for the TCA cycle, and it reversibly converts citrate to isocitrate, maintains mitochondrial function, and regulates metabolism.[29] Dysregulated ACO2 is associated with oxidant-/lipopolysaccharide-induced mtDNA damage and apoptosis.[42,43] Our results consistently revealed that ACO2 downregulation mediated by NR1D1 decreased mitochondrial respiratory capacity, increased mtDNA damage, reduced mitochondrial membrane potential, and aggravated mitochondria-mediated apoptosis in VSMCs. These data provided novel evidence supporting a role of the mitochondrial TCA cycle in the pathogenesis of AAAs, and identified the NR1D1-ACO2 axis as a potential novel target for regulating mitochondrial metabolism and function in AAA treatment.

TCA cycle metabolites are important for the biosynthesis of macromolecules, such as nucleotides, lipids, and proteins, and are involved in physiology and disease.[31] Recent evidence revealed several new and important roles for TCA cycle intermediates as signaling molecules, gene expression effectors, and stress response modulators in controlling cellular function and fate.[31] As the downstream factor of mitochondrial

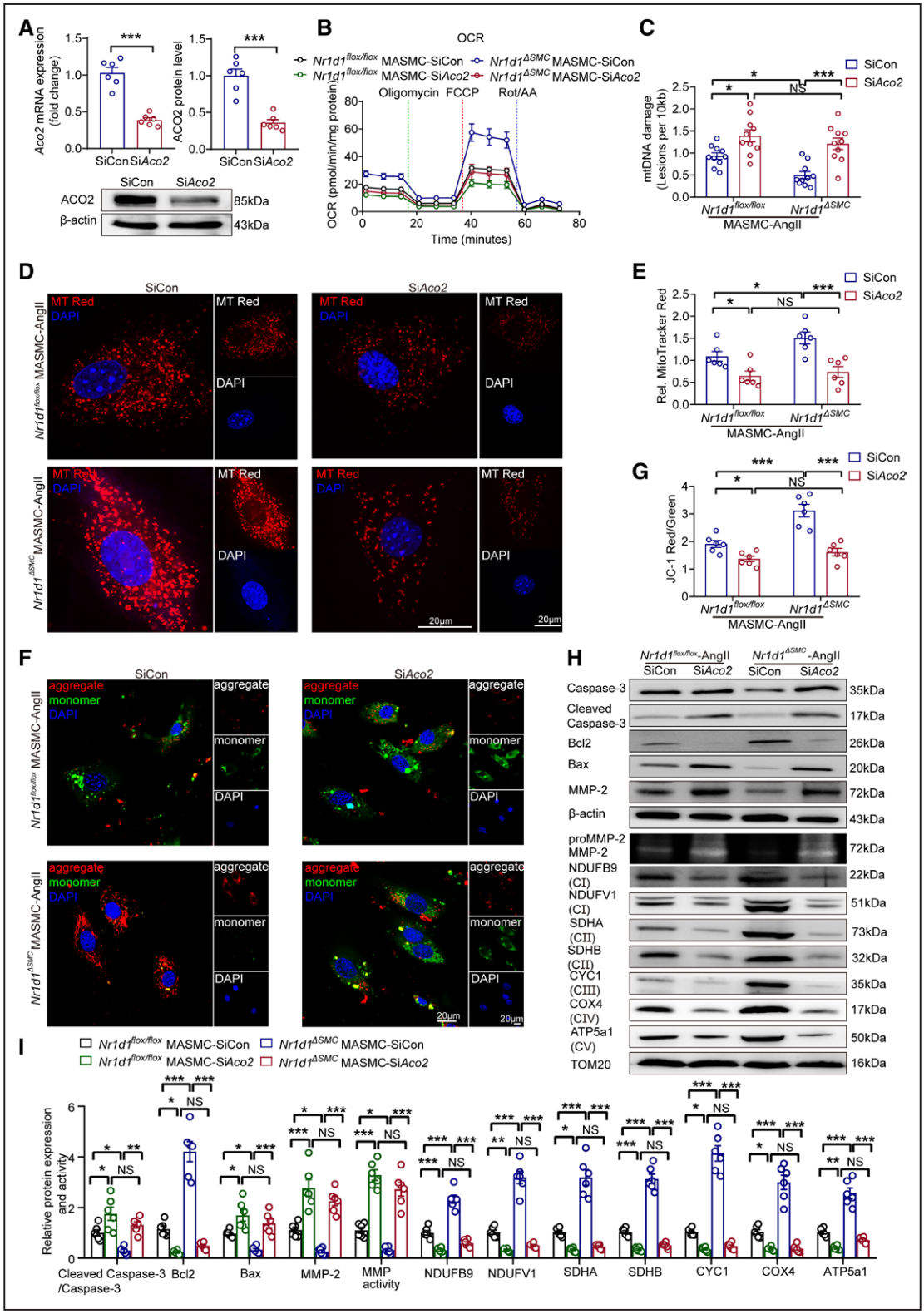

Figure 7. ACO2 silencing abolishes the protective effects of NR1D1 deficiency on mitochondrial function.
A, **Top**, Quantification of *Aco2* mRNA and ACO2 protein expression assessed by RT-qPCR and Western blot in MASMCs after transfection with SiCon and Si*Aco2*-1, normalized to *β-actin* (n=6 independent experiments). Data were analyzed by Student *t* test. ***$P<0.001$. **Botto**m, ACO2 protein expression assessed by Western blot in indicated groups. **B**, Summarized OCR tracings in AngII-treated MASMCs isolated from *Nr1d1*$^{flox/flox}$ and *Nr1d1*$^{\Delta SMC}$ mice pretreated with SiCon and Si*Aco2* (n=6 independent experiments). **C**, mtDNA damage assay in indicated groups (n=10 independent experiments). Data were analyzed by 2-way ANOVA followed by the Bonferroni post hoc test. *$P<0.05$; ***$P<0.001$. **D**, MitoTracker Red CMXRos staining was used to measure mitochondrial membrane potential for the assessment of early-stage apoptosis. (*Continued*)

Figure 7 Continued. E, Quantification of MitoTracker Red CMXRos staining (n=6 independent experiments). Data were analyzed by 2-way ANOVA followed by the Bonferroni post hoc test. *P<0.05; ***P<0.001. **F**, JC-1 staining was used to measure mitochondrial membrane potential for the assessment of early-stage apoptosis. **G**, Quantification of JC-1 staining (n=6 independent experiments). Data were analyzed by 2-way ANOVA followed by the Bonferroni post hoc test. *P<0.05; ***P<0.001. **H**, Protein expression of MMP-2, apoptotic proteins (Cleaved caspase-3/Caspase-3, Bcl2 and Bax), and mitochondrial ETC complexes measured by Western blot, and MMP activity determined by zymography in indicated groups. **I**, Quantification of MMP-2, apoptotic proteins (Cleaved caspase-3/Caspase-3, Bcl2 and Bax), and mitochondrial ETC complexes protein expression determined by Western blot and MMP activity determined by zymography in indicated groups (n=6 independent experiments). Data were analyzed by 2-way ANOVA followed by the Bonferroni post hoc test. *P<0.05; **P<0.01; ***P<0.001. Data are expressed as mean ± SEM. ACO2 indicates aconitase-2; AngII, angiotensin II; ETC, electron transport chain; MASMC, mouse aortic smooth muscle cell; MMP, matrix metallopeptidase; mtDNA, mitochondrial DNA; NR1D1, nuclear receptor subfamily 1 group D member 1; NS, nonsignificant; OCR, oxygen consumption rate; and RT-qPCR, real-time quantitative polymerase chain reaction.

ACO2, αKG is regarded as a crucial intermediate in the TCA cycle, and its pleiotropic effects are connected to its antioxidant and anti-aging properties as a signaling molecule.[44] Dietary αKG not only improves energy metabolism, extends lifespan, and reduces morbidity in aging mice[45] but also exhibits protective effects on cardiac surgery and mitochondrial myopathies.[44,46] In the present study, supplementation with exogenous αKG significantly improved mitochondrial function and reversed AAA development in both AngII- and $CaPO_4$-induced AAA models. Our data provide valuable insights into the biological action of αKG in AAA prevention and treatment. It is interesting that a recent publication reported that the TCA cycle metabolite succinate had detrimental effects on the development of aortic dissections and aneurysms.[47] In contrast with our study, Cui et al[47] enrolled patients with both thoracic and abdominal aortic diseases, including aortic dissections and aneurysms. Although the physical appearance of thoracic and abdominal aortic diseases is similar, there are distinct differences with respect to the embryonic origin of the thoracic aorta and abdominal aorta, resulting in different disease pathologies.[48] Moreover, aortic dissections and aortic aneurysms are distinct diseases with clear differences in pathological changes and cellular mechanisms.[49] The different roles of the TCA cycle metabolites α-KG and succinate in aortic diseases deserve further research.

Up to now, 49 members of the NR superfamily have been documented;[25] however, the role of most NRs in AAA remains unknown. In a recent study, we found that NR4A1, an orphan member of the metabolic NR superfamily, acted as a negative regulator of AAA pathology by targeting inflammation in macrophages.[19] The present study adds novel evidence that NR1D1, the top-ranked metabolic NR in gene expression fold change in AAA tissues, acts as an endogenous positive regulator contributing to the AAA pathogenesis by targeting the VSMC mitochondrial TCA cycle. Given the distinct regulatory roles of these metabolic NRs in AAA injury, potential regulatory cross-talk among them might maintain the delicate homeostatic balance between cell death and survival in AAA development. Characterization of the molecular cross-talk between these metabolic NR pathways is a prerequisite for a complete understanding of AAA pathological processes.

CLINICAL IMPLICATIONS OF THIS STUDY

The identification of NR1D1 as a novel functional receptor in mitochondrial metabolism regulation in vascular cells might broaden our understanding of the multiple biological functions of NR1D1.[38] Our observations, along with recent findings about the role of NR1D1 in cardiovascular tissues from several research groups,[8,9,12,50] provide support for NR1D1 as an essential regulator of cardiovascular biology. It is important that our study unveils a previously undescribed NR1D1-ACO2-αKG axis in regulating mitochondrial metabolism, and provides proof-of-concept evidence indicating the therapeutic value of αKG supplementation in AAA prevention and treatment. αKG is a biological compound found naturally in the human body and available in dietary supplement form. On this basis of these findings, we initiated a prospective, randomized, parallel-group, controlled study to assess the efficacy and safety of αKG in patients with AAA (Alpha-Ketoglutarate in Abdominal Aortic Aneurysm, 4A Study; Registration: https://www.clinicaltrials.gov; Unique identifier: NCT04723888).

Limitations of the Study

Several study limitations should be considered. First, although a detrimental role of NR1D1 in AAA has been confirmed in our study in 2 AAA mouse models (subcutaneous AngII infusion and adventitial $CaPO_4$ incubation) using both global and conditional knockout mice, each animal model is limited in its ability to mimic the extremely complex process of AAA formation in patients. In addition, although *Tagln-Cre* drivers have been commonly used to study VSMC-specific expression, findings with this strain need to be interpreted with caution because its VSMC specificity is controversial.[51] Second, the human AAA tissues obtained from advanced AAA lesions during open surgical repair provide limited insight into the earlier stages. Third, the mechanism underlying the discrepancy between our findings (detrimental effect of NR1D1 on AAA) and previous reports (protective effects of NR1D1 on atherosclerosis) remains unclear. Whether this discrepancy is a result of the distinct roles in different vascular cell types induced by various pathological stimuli must be further defined. Last, our findings highlight αKG supplementation as a potential treatment for

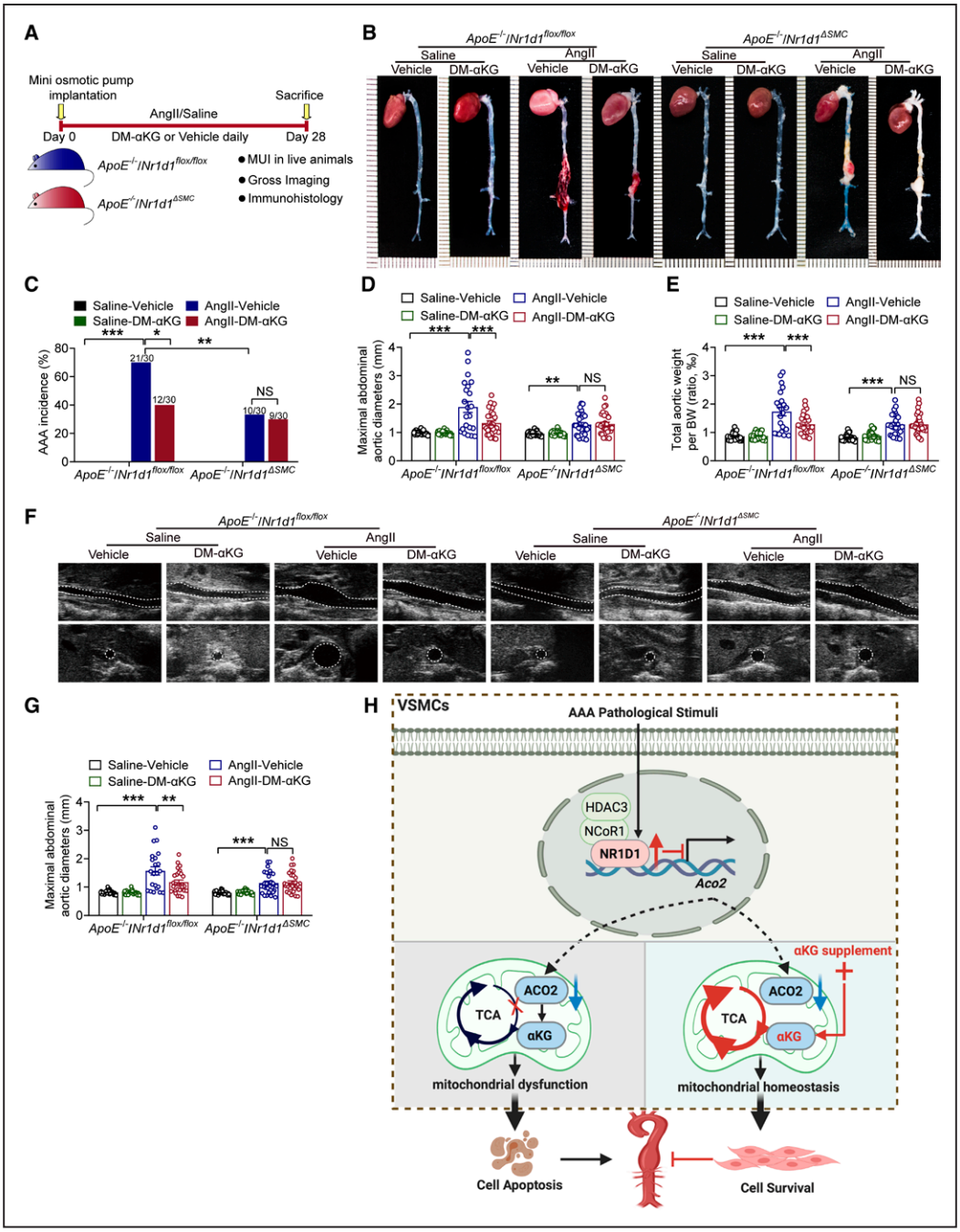

Figure 8. Supplementation with the ACO2 downstream metabolite αKG protects against AAA formation.
A, Schematic protocol: saline- or AngII-infused *ApoE*$^{-/-}$/*Nr1d1*$^{flox/flox}$ and *ApoE*$^{-/-}$/*Nr1d1*$^{\Delta SMC}$ mice were intraperitoneally injected with vehicle or DM-αKG (100 mg/kg/d) for 28 days. **B**, Representative images of the macroscopic features of AAA formation in indicated groups. **C**, The incidence of AAA formation in indicated groups (n=30 per group). Data were analyzed by a Fisher exact test. *P<0.05; **P<0.01; ***P<0.001. **D**, Quantification of the maximal diameter of suprarenal abdominal aortas measured using a Digital Vernier Caliper (n=22–30 per group). Data were analyzed by 2-way ANOVA followed by the Bonferroni post hoc test. **P<0.01; ***P<0.001. **E**, Quantification of total aortic weight/BW (n=22–30 per group). Data were analyzed by 2-way ANOVA followed by the Bonferroni post hoc test. ***P<0.001. **F**, Representative images of suprarenal abdominal aortas visualized by MUI using the B mode in indicated groups. **G**, Quantification of the maximal diameter of suprarenal abdominal aortas measured by MUI using the B mode in indicated groups (n=22–30 per group). Data were analyzed by 2-way ANOVA followed by the Bonferroni post hoc test. **P<0.01; ***P<0.001. Data are expressed as mean ± SEM. **H**, Schematic representation of the molecular mechanisms. Under a pathological state during AAA development, upregulation of NR1D1 represses the nuclear transcription of *Aco2* in VSMCs with recruitment of the NCoR1-HDAC3 corepressor complex. Consequently, reduced ACO2 expression and activity suppress the TCA cycle, disrupt mitochondrial homeostasis, and subsequently trigger VSMCs apoptosis, eventually resulting in the formation of AAA. Supplementation with αKG, a downstream metabolite of ACO2, alleviates mitochondrial dysfunction and restricts AAA formation. AAA indicates abdominal aortic aneurysm; ACO2, aconitase-2; αKG, α-ketoglutarate; AngII, angiotensin II; DM-αKG, dimethyl α-ketoglutarate; HDAC3, histone deacetylase 3; MUI, micro-ultrasound imaging; NCoR1, nuclear receptor corepressor 1; NR1D1, nuclear receptor subfamily 1 group D member 1; NS, nonsignificant; SMC, smooth muscle cell; TCA, tricarboxylic acid; and VSMCs, vascular smooth muscle cells.

AAA. More clinical research is warranted to confirm the benefit on AAA observed in this study.

ARTICLE INFORMATION

Received September 21, 2021; accepted June 10, 2022.

Affiliations

State Key Laboratory for Oncogenes and Related Genes, Department of Cardiology (L.-Y.S., Y.-Y.L., H.-Y.Z., Z.S., G.-Q.L., N.G., Z.-H.F., X.G., N.L., S.D., A.-C.Y., J.P.), Department of Vascular Surgery (Y.-L.W., L.Z.), Renji Hospital, School of Medicine, School of Biomedical Engineering and Med-X Research Institute (L.H., K.Q.), Shanghai Jiao Tong University, Shanghai, China.

Acknowledgments

The authors thank Dr Ueli Schibler (University of Geneva, Geneva, Switzerland) for providing global *Nr1d1* knockout mice. The authors thank Professor Hou-Zao Chen from the Chinese Academy of Medical Sciences for his critical comments on this article. J.P. designed the study and supervised data analysis; L.-Y.S., Y.-Y.L., H.-Y.Z., Z.S., N.G., Y.-L.W., Z.-H.F., N.L., G.-Q.L., X.G., S.D., and A.-C.Y. conducted the biochemical experiments; L.-Y.S., Y.-Y.L., Y.-L.W., L.H., L.Z., K.Q., and J.P. designed the metabolomics studies and contributed to data interpretation; A.-C.Y. conducted the echocardiographic analysis; L.-Y.S. and Y.-Y.L. analyzed the data and prepared the figures; L.-Y.S. and Y.-Y.L. wrote the article; J.P. reviewed and edited the article.

Sources of Funding

This work was supported by grants from the National Science Fund for Distinguished Young Scholars (81625002), National Natural Science Foundation of China (81930007, 82230014, 81800048, 81800378, 82070477, and 91839301), Shanghai Science and Technology Committee (19ZR1430400 and 22JC1402100), Innovative Research Team of High-Level Local Universities in Shanghai, and Shanghai Municipal Key Clinical Specialty (shslczdzk06204).

Disclosures

None.

Supplemental Material

Expanded Methods

Expanded Results

Tables S1–S4

Figures S1–S18

REFERENCES

1. Chaikof EL, Dalman RL, Eskandari MK, Jackson BM, Lee WA, Mansour MA, Mastracci TM, Mell M, Murad MH, Nguyen LL, et al. The Society for Vascular Surgery practice guidelines on the care of patients with an abdominal aortic aneurysm. *J Vasc Surg.* 2018;67:2–77.e2. doi: 10.1016/j.jvs.2017.10.044
2. Shi J, Yang Y, Cheng A, Xu G, He F. Metabolism of vascular smooth muscle cells in vascular diseases. *Am J Physiol Heart Circ Physiol.* 2020;319:H613–H631. doi: 10.1152/ajpheart.00220.2020
3. Nasrallah CM, Horvath TL. Mitochondrial dynamics in the central regulation of metabolism. *Nat Rev Endocrinol.* 2014;10:650–658. doi: 10.1038/nrendo.2014.160
4. Li Y, Ren P, Dawson A, Vasquez HG, Ageedi W, Zhang C, Luo W, Chen R, Li Y, Kim S, et al. Single-cell transcriptome analysis reveals dynamic cell populations and differential gene expression patterns in control and aneurysmal human aortic tissue. *Circulation* 2020;142:1374–1388. doi: 10.1161/CIRCULATIONAHA.120.046528
5. Hollenberg AN. Metabolic health and nuclear-receptor sensitivity. *N Engl J Med.* 2012;366:1345–1347. doi: 10.1056/NEJMcibr1114529
6. De Bosscher K, Desmet SJ, Clarisse D, Estebanez-Perpina E, Brunsveld L. Nuclear receptor crosstalk - defining the mechanisms for therapeutic innovation. *Nat Rev Endocrinol.* 2020;16:363–377. doi: 10.1038/s41574-020-0349-5
7. Lazar MA, Hodin RA, Darling DS, Chin WW. A novel member of the thyroid/steroid hormone receptor family is encoded by the opposite strand of the rat c-erbA alpha transcriptional unit. *Mol Cell Biol.* 1989;9:1128–1136. doi: 10.1128/mcb.9.3.1128-1136.1989
8. Shi J, Tong R, Zhou M, Gao Y, Zhao Y, Chen Y, Liu W, Li G, Lu D, Meng G, et al. Circadian nuclear receptor Rev-erbα is expressed by platelets and potentiates platelet activation and thrombus formation. *Eur Heart J.* 2022;43:2317–2334. doi: 10.1093/eurheartj/ehac109
9. Zhao Y, Lu X, Wan F, Gao L, Lin N, He J, Wei L, Dong J, Qin Z, Zhong F, et al. Disruption of circadian rhythms by shift work exacerbates reperfusion injury in myocardial infarction. *J Am Coll Cardiol.* 2022;79:2097–2115. doi: 10.1016/j.jacc.2022.03.370
10. Hunter AL, Pelekanou CE, Adamson A, Downton P, Barron NJ, Cornfield T, Poolman TM, Humphreys N, Cunningham PS, Hodson L, et al. Nuclear receptor REVERBα is a state-dependent regulator of liver energy metabolism. *Proc Natl Acad Sci USA.* 2020;117:25869–25879. doi: 10.1073/pnas.2005330117
11. Dashti HS, Follis JL, Smith CE, Tanaka T, Garaulet M, Gottlieb DJ, Hruby A, Jacques PF, Kiefte-de Jong JC, Lamon-Fava S, et al. Gene-environment interactions of circadian-related genes for cardiometabolic traits. *Diabetes Care.* 2015;38:1456–1466. doi: 10.2337/dc14-2709
12. Montaigne D, Marechal X, Modine T, Coisne A, Mouton S, Fayad G, Ninni S, Klein C, Ortmans S, Seunes C, et al. Daytime variation of perioperative myocardial injury in cardiac surgery and its prevention by Rev-erbα antagonism: a single-centre propensity-matched cohort study and a randomised study. *Lancet.* 2018;391:59–69. doi: 10.1016/S0140-6736(17)32132-3
13. Wu Z, Liao F, Luo G, Qian Y, He X, Xu W, Ding S, Pu J. NR1D1 deletion induces rupture-prone vulnerable plaques by regulating macrophage pyroptosis via the NF-κB/NLRP3 inflammasome pathway. *Oxid Med Cell Longev.* 2021;2021:5217572. doi: 10.1155/2021/5217572
14. Zhao G, Fu Y, Cai Z, Yu F, Gong Z, Dai R, Hu Y, Zeng L, Xu Q, Kong W. Unspliced XBP1 confers VSMC homeostasis and prevents aortic aneurysm formation via FoxO4 interaction. *Circ Res.* 2017;121:1331–1345. doi: 10.1161/CIRCRESAHA.117.311450
15. Preitner N, Damiola F, Lopez-Molina L, Zakany J, Duboule D, Albrecht U, Schibler U. The orphan nuclear receptor Rev-erbalpha controls circadian transcription within the positive limb of the mammalian circadian oscillator. *Cell.* 2002;110:251–260. doi: 10.1016/s0092-8674(02)00825-5
16. Zhang Y, Da Q, Cao S, Yan K, Shi Z, Miao Q, Li C, Hu L, Sun S, Wu W, et al. HINT1 (histidine triad nucleotide-binding protein 1) attenuates cardiac hypertrophy via suppressing HOXA5 (homeobox a5) expression. *Circulation.* 2021;144:638–654. doi: 10.1161/CIRCULATIONAHA.120.051094
17. Chen HZ, Wang F, Gao P, Pei JF, Liu Y, Xu TT, Tang X, Fu WY, Lu J, Yan YF, et al. Age-associated sirtuin 1 reduction in vascular smooth muscle links vascular senescence and inflammation to abdominal aortic aneurysm. *Circ Res.* 2016;119:1076–1088. doi: 10.1161/CIRCRESAHA.116.308895
18. Hsu PL, Chen JS, Wang CY, Wu HL, Mo FE. Shear-induced CCN1 promotes atheroprone endothelial phenotypes and atherosclerosis. *Circulation.* 2019;139:2877–2891. doi: 10.1161/CIRCULATIONAHA.118.033895
19. Zhang H, Geng N, Sun L, Che X, Xiao Q, Tao Z, Chen L, Lyu Y, Shao Q, Pu J. Nuclear receptor Nur77 protects against abdominal aortic aneurysm by ameliorating inflammation via suppressing LOX-1. *J Am Heart Assoc.* 2021;10:e021707. doi: 10.1161/JAHA.121.021707
20. Salmon M, Johnston WF, Woo A, Pope NH, Su G, Upchurch GR Jr, Owens GK, Ailawadi G. KLF4 regulates abdominal aortic aneurysm morphology and deletion attenuates aneurysm formation. *Circulation.* 2013;128:S163–S174. doi: 10.1161/CIRCULATIONAHA.112.000238
21. Xu L, Su Y, Zhao Y, Sheng X, Tong R, Ying X, Gao L, Ji Q, Gao Y, Yan Y, et al. Melatonin differentially regulates pathological and physiological cardiac hypertrophy: crucial role of circadian nuclear receptor RORα signaling. *J Pineal Res.* 2019;67:e12579. doi: 10.1111/jpi.12579
22. Satoh K, Nigro P, Matoba T, O'Dell MR, Cui Z, Shi X, Mohan A, Yan C, Abe J, Illig KA, et al. Cyclophilin A enhances vascular oxidative stress and the development of angiotensin II-induced aortic aneurysms. *Nat Med.* 2009;15:649–656. doi: 10.1038/nm.1958
23. Brumbaugh CD, Kim HJ, Giovacchini M, Pourmand N. NanoStriDE: normalization and differential expression analysis of NanoString nCounter data. *BMC Bioinf.* 2011;12:479. doi: 10.1186/1471-2105-12-479
24. Wei X, Liu Z, Jin X, Huang L, Gurav DD, Sun X, Liu B, Ye J, Qian K. Plasmonic nanoshells enhanced laser desorption/ionization mass spectrometry for detection of serum metabolites. *Anal Chim Acta.* 2017;950:147–155. doi: 10.1016/j.aca.2016.11.017
25. Evans RM, Mangelsdorf DJ. Nuclear receptors, RXR, and the big bang. *Cell.* 2014;157:255–266. doi: 10.1016/j.cell.2014.03.012
26. Cheng Z, Volkers M, Din S, Avitabile D, Khan M, Gude N, Mohsin S, Bo T, Truffa S, Alvarez R, et al. Mitochondrial translocation of Nur77 mediates cardiomyocyte apoptosis. *Eur Heart J.* 2011;32:2179–2188. doi: 10.1093/eurheartj/ehq496

27. Pu J, Yuan A, Shan P, Gao E, Wang X, Wang Y, Lau WB, Koch W, Ma XL, He B. Cardiomyocyte-expressed farnesoid-X-receptor is a novel apoptosis mediator and contributes to myocardial ischaemia/reperfusion injury. *Eur Heart J.* 2013;34:1834–1845. doi: 10.1093/eurheartj/ehs011
28. Chong J, Soufan O, Li C, Caraus I, Li S, Bourque G, Wishart DS, Xia J. MetaboAnalyst 4.0: towards more transparent and integrative metabolomics analysis. *Nucleic Acids Res.* 2018;46:W486–W494. doi: 10.1093/nar/gky310
29. Palmieri EM, Gonzalez-Cotto M, Baseler WA, Davies LC, Ghesquiere B, Maio N, Rice CM, Rouault TA, Cassel T, Higashi RM, et al. Nitric oxide orchestrates metabolic rewiring in M1 macrophages by targeting aconitase 2 and pyruvate dehydrogenase. *Nat Commun.* 2020;11:698. doi: 10.1038/s41467-020-14433-7
30. Kim YH, Marhon SA, Zhang Y, Steger DJ, Won KJ, Lazar MA. Rev-erbα dynamically modulates chromatin looping to control circadian gene transcription. *Science.* 2018;359:1274–1277. doi: 10.1126/science.aao6891
31. Martinez-Reyes I, Chandel NS. Mitochondrial TCA cycle metabolites control physiology and disease. *Nat Commun.* 2020;11:102. doi: 10.1038/s41467-019-13668-3
32. Elia I, Rossi M, Stegen S, Broekaert D, Doglioni G, van Gorsel M, Boon R, Escalona-Noguero C, Torrekens S, Verfaillie C, et al. Breast cancer cells rely on environmental pyruvate to shape the metastatic niche. *Nature.* 2019;568:117–121. doi: 10.1038/s41586-019-0977-x
33. Rateri DL, Howatt DA, Moorleghen JJ, Charnigo R, Cassis LA, Daugherty A. Prolonged infusion of angiotensin II in apoE(-/-) mice promotes macrophage recruitment with continued expansion of abdominal aortic aneurysm. *Am J Pathol.* 2011;179:1542–1548. doi: 10.1016/j.ajpath.2011.05.049
34. Lonard DM, O'Malley BW. Nuclear receptor coregulators: modulators of pathology and therapeutic targets. *Nat Rev Endocrinol.* 2012;8:598–604. doi: 10.1038/nrendo.2012.100
35. Yin L, Wu N, Curtin JC, Qatanani M, Szwergold NR, Reid RA, Waitt GM, Parks DJ, Pearce KH, Wisely GB, et al. Rev-erbalpha, a heme sensor that coordinates metabolic and circadian pathways. *Science.* 2007;318:1786–1789. doi: 10.1126/science.1150179
36. Zhang Y, Fang B, Emmett MJ, Damle M, Sun Z, Feng D, Armour SM, Remsberg JR, Jager J, Soccio RE, et al. GENE REGULATION. Discrete functions of nuclear receptor Rev-erbα couple metabolism to the clock. *Science.* 2015;348:1488–1492. doi: 10.1126/science.aab3021
37. Gerhart-Hines Z, Lazar MA. Rev-erbα and the circadian transcriptional regulation of metabolism. *Diabetes Obes Metab.* 2015;17:12–16. doi: 10.1111/dom.12510
38. Woldt E, Sebti Y, Solt LA, Duhem C, Lancel S, Eeckhoute J, Hesselink MK, Paquet C, Delhaye S, Shin Y, et al. Rev-erb-α modulates skeletal muscle oxidative capacity by regulating mitochondrial biogenesis and autophagy. *Nat Med.* 2013;19:1039–1046. doi: 10.1038/nm.3213
39. Cho H, Zhao X, Hatori M, Yu RT, Barish GD, Lam MT, Chong LW, DiTacchio L, Atkins AR, Glass CK, et al. Regulation of circadian behaviour and metabolism by REV-ERB-α and REV-ERB-β. *Nature.* 2012;485:123–127. doi: 10.1038/nature11048
40. Zhang GF, Jensen MV, Gray SM, El K, Wang Y, Lu D, Becker TC, Campbell JE, Newgard CB. Reductive TCA cycle metabolism fuels glutamine- and glucose-stimulated insulin secretion. *Cell Metab.* 2021;33:804–817.e5. doi: 10.1016/j.cmet.2020.11.020
41. Cai Z, Li CF, Han F, Liu C, Zhang A, Hsu CC, Peng D, Zhang X, Jin G, Rezaeian AH, et al. Phosphorylation of PDHA by AMPK drives TCA cycle to promote cancer metastasis. *Mol Cell.* 2020;80:263–278.e7. doi: 10.1016/j.molcel.2020.09.018
42. Kim SJ, Cheresh P, Williams D, Cheng Y, Ridge K, Schumacker PT, Weitzman S, Bohr VA, Kamp DW. Mitochondria-targeted Ogg1 and aconitase-2 prevent oxidant-induced mitochondrial DNA damage in alveolar epithelial cells. *J Biol Chem.* 2014;289:6165–6176. doi: 10.1074/jbc.M113.515130
43. Guo J, Xing H, Chen M, Wang W, Zhang H, Xu S. H2S inhalation-induced energy metabolism disturbance is involved in LPS mediated hepatocyte apoptosis through mitochondrial pathway. *Sci Total Environ.* 2019;663:380–386. doi: 10.1016/j.scitotenv.2019.01.360
44. Bayliak MM, Lushchak VI. Pleiotropic effects of alpha-ketoglutarate as a potential anti-ageing agent. *Ageing Res Rev.* 2020;66:101237. doi: 10.1016/j.arr.2020.101237
45. Asadi Shahmirzadi A, Edgar D, Liao CY, Hsu YM, Lucanic M, Asadi Shahmirzadi A, Wiley CD, Gan G, Kim DE, Kasler HG, et al. Alpha-ketoglutarate, an endogenous metabolite, extends lifespan and compresses morbidity in aging mice. *Cell Metab.* 2020;32:447456.e6. doi: 10.1016/j.cmet.2020.08.004
46. Chen Q, Kirk K, Shurubor YI, Zhao D, Arreguin AJ, Shahi I, Valsecchi F, Primiano G, Calder EL, Carelli V, et al. Rewiring of glutamine metabolism is a bioenergetic adaptation of human cells with mitochondrial DNA mutations. *Cell Metab.* 2018;27:1007–1025.e5. doi: 10.1016/j.cmet.2018.03.002
47. Cui H, Chen Y, Li K, Zhan R, Zhao M, Xu Y, Lin Z, Fu Y, He Q, Tang PC, et al. Untargeted metabolomics identifies succinate as a biomarker and therapeutic target in aortic aneurysm and dissection. *Eur Heart J.* 2021;42:4373–4385. doi: 10.1093/eurheartj/ehab605
48. Majesky MW. Developmental basis of vascular smooth muscle diversity. *Arterioscler Thromb Vasc Biol.* 2007;27:1248–1258. doi: 10.1161/ATVBAHA.107.141069
49. Quintana RA, Taylor WR. Cellular mechanisms of aortic aneurysm formation. *Circ Res.* 2019;124:607–618. doi: 10.1161/CIRCRESAHA.118.313187
50. Reitz CJ, Alibhai FJ, Khatua TN, Rasouli M, Bridle BW, Burris TP, Martino TA. SR9009 administered for one day after myocardial ischemia-reperfusion prevents heart failure in mice by targeting the cardiac inflammasome. *Commun Biol.* 2019;2:353. doi: 10.1038/s42003-019-0595-z
51. Chakraborty R, Saddouk FZ, Carrao AC, Krause DS, Greif DM, Martin KA. Promoters to study vascular smooth muscle. *Arterioscler Thromb Vasc Biol.* 2019;39:603–612. doi: 10.1161/ATVBAHA.119.312449